

**SOUND-SIDE LIMB GAIT ANALYSIS USING  
MACHINE LEARNING IN LOWER LIMB PROSTHESIS**

A Dissertation  
Presented to  
The Academic Faculty

by

Jeongwoo Cho

In Partial Fulfillment  
of the Requirements for the Degree  
Master of Science Mechanical Engineering in the  
George W. Woodruff School of Mechanical Engineering

Georgia Institute of Technology  
August 2024

**COPYRIGHT © 2024 BY JEONGWOO CHO**

**SOUND-SIDE LIMB GAIT ANALYSIS USING  
MACHINE LEARNING IN LOWER LIMB PROSTHESIS**

Approved by:

Dr. Aaron J. Young, Advisor  
School of Mechanical Engineering  
*Georgia Institute of Technology*

Dr. Gregory Sawicki  
School of Mechanical Engineering  
*Georgia Institute of Technology*

Kinsey Herrin  
School of Mechanical Engineering  
*Georgia Institute of Technology*

Date Approved: July 11, 2024

## ACKNOWLEDGEMENTS

I would like to thank Dr. Young for his guidance and support throughout this whole thesis process. He provided me with the opportunity to conduct research in robotics and I have gained so much experience and knowledge during the past five years at the EPIC Lab.

I would like to thank Jairo Maldonado-Contreras for being an amazing mentor throughout my entire undergrad and Master's. His constant help and advice have helped me feel more comfortable exploring and researching new ideas. I would also like to thank Jason Zhou for his immense knowledge in VICON and OpenSim. Without him this project would genuinely not have been possible.

I would also like to thank all other past and current graduate and undergraduate members from the prosthesis team that I have worked with throughout the years. You have all made the lab feel like a second home and is the reason why I fell in love with doing research.

Finally, special thanks to my parents, brother, and girlfriend. Their sacrifices and support have made me who I am now, and without them I would not have had such an invaluable opportunity. Thank you for always being there for me and inspiring me to be a better version of myself every day.

# TABLE OF CONTENTS

<b>Acknowledgements</b>	<b>iv</b>
<b>List of Tables</b>	<b>vii</b>
<b>List of Figures</b>	<b>viii</b>
<b>List of Abbreviations</b>	<b>xi</b>
<b>Summary</b>	<b>xii</b>
<b>Chapter 1: Introduction and Background</b>	<b>1</b>
1.1 Sensing on Powered Prosthesis	2
1.2 Machine Learning for Prosthesis Control	2
1.3 Gait Symmetry Measurement	4
1.4 Novelty of Work	5
<b>Chapter 2: Open Source Leg</b>	<b>8</b>
2.1 Onboard Sensors and Actuators	8
2.2 Controller Design	9
2.2.1 High-level controller	9
2.2.2 Mid-level controller	10
2.2.3 Low-level controller	11
<b>Chapter 3: Methodology and Machine Learning Model Design</b>	<b>12</b>
3.1 Experiment Protocol	12
3.1.1 Biomechanics Processing	14

3.1.2	Sound-side Sensor Simulation	15
3.1.3	Data Pre-processing for Machine Learning	16
3.2	Machine Learning Models	17
3.2.1	Convolutional Neural Network (CNN)	17
3.2.2	Temporal Convolutional Network (TCN)	20
3.2.3	Model Hyperparameter Optimization and Training	22
3.2.4	Joint Work Analysis	24
3.2.5	Work Correlation Coefficient Analysis	25
3.2.6	Statistical Analysis	26
<b>Chapter 4:</b>	<b>Results</b>	<b>27</b>
4.1	Inter-Joint Estimation Model Comparison	28
4.1.1	CNN Power to Work Integration Model	30
4.2	Sound-Side Sensor-Set Optimization	31
4.3	Multi-Modal Estimation	33
4.3.1	Combined LW and Ramps CNN	34
4.3.2	Sound-side sensor sweep for ramps	36
<b>Chapter 5:</b>	<b>Discussion</b>	<b>39</b>
<b>Chapter 6:</b>	<b>Conclusion and Future Work</b>	<b>44</b>
<b>References</b>		<b>46</b>

## LIST OF TABLES

Table 1. CNN hyperparameters and training. ....	22
Table 2. TCN hyperparameters.....	23

## LIST OF FIGURES

Figure 1. Open-Source Leg (OSL) onboard sensors.....	8
Figure 2. OSL hierarchical control structure. ....	10
Figure 3. Terrain park used for various experimental protocols. VICON system allows for motion-capturing capabilities and force plates make it possible to calculate ground reaction forces as the user ambulates around the park. ....	12
Figure 4. Musculoskeletal model of a subject in OpenSim on left and motion capture makers in VICON software on right. ....	14
Figure 5. Simulated IMU and foot insole location and axes.....	16
Figure 6. Overview of a CNN architecture and data transformation [57]. ....	18
Figure 7. (a) CNN for joint power estimation (b) CNN for joint work estimation.....	19
Figure 8. Convolutional dilation in a TCN [56]. ....	20
Figure 9. Residual block connection in a TCN [55]. ....	21

Figure 10. Visualization of the joint power curves of each of the intact joints for different locomotion modes. The plots show averaged joint power over all collected gait cycles for one random subject and the associated standard deviation. The same subject is shown across all modes and joints.....	24
Figure 11. Comparison of ML models' performances in estimating each of the joint work. Sound joints are trained and estimated using full sound-side sensors, while prosthesis joints use only prosthesis sensors. Error bars represent $\pm 1$ standard deviation across all subjects and asterisks indicate statistical significance ( $p < 0.05$ ). .....	28
Figure 12. Sensor variation on each joint work estimation in level walking using CNN-power model (above) and CNN-work model (below). Error bars represent $\pm 1$ standard deviation across all subjects ( $N=7$ ) and asterisks indicate statistical significance ( $p < 0.05$ ). .....	30
Figure 13. Sound-side sensor subset comparison using the CNN-power model on sound-side joints. Error bars represent $\pm 1$ standard deviation across all subjects ( $N=7$ ) and asterisks indicate statistical significance ( $p < 0.05$ ). .....	32
Figure 14. Combined LW and ramps CNN-power model for estimating each of the joint works. Sound joints are trained and estimated using full sound-side sensors, while prosthesis joints use only prosthesis sensors. Error bars represent $\pm 1$ standard deviation across all subjects ( $N=7$ for ramps and $N=7$ for level walking) and asterisks indicate statistical significance ( $p < 0.05$ ).....	34
Figure 15. Inter-limb joint power estimation in ramp ascent positive work (left) and ramp descent negative work (right) correlations. The CNN-power model trained on both level walking and ramp trials. Error bars represent $\pm 1$ standard deviation across all subjects ( $N=7$ ) and asterisks indicate statistical significance ( $p < 0.05$ ). .....	35

Figure 16. Sound-side sensor subset comparison using a level-walking and ramp trained CNN-power model on sound-side ankle joint during ramp ascent (left) and ramp descent (right). Error bars represent  $\pm 1$  standard deviation across all subjects (N=7)..... 37

Figure 17. Sound-side sensor subset comparison using a level-walking and ramp trained CNN-power model on the sound-side knee joint during ramp ascent (left) and ramp descent (right). Error bars represent  $\pm 1$  standard deviation across all subjects (N=7)..... 37

Figure 18. Sound-side sensor subset comparison using a level-walking and ramp trained CNN-power model on the sound-side hip joint during ramp ascent (left) and ramp descent (right). Error bars represent  $\pm 1$  standard deviation across all subjects..... 38

## LIST OF ABBREVIATIONS

<b>AB</b>	Able body
<b>CNN</b>	Convolutional Neural Network
<b>FSM</b>	Finite State Machine
<b>GRF</b>	Ground Reaction Force
<b>IMU</b>	Inertial Measurement Unit
<b>LW</b>	Level Walking
<b>ML</b>	Machine Learning
<b>NN</b>	Neural Network
<b>OSL</b>	Open-Source Leg
<b>RA</b>	Ramp Ascent
<b>RD</b>	Ramp Descent
<b>TCN</b>	Temporal Convolutional Network
<b>TF</b>	Transfemoral

## SUMMARY

Unilateral lower limb amputees face a higher risk of joint degradation due to uneven loads while walking. Existing research often focuses on joint moment predictions but lacks comprehensive assessment of joint work, which is crucial for understanding energy dynamics and joint health. This thesis addresses this gap by developing and validating a machine learning pipeline to estimate joint work from onboard prosthesis sensors, eliminating the need for external devices. Our approach provides a joint estimation method that can be used to optimize prosthetic assistance and promote healthier gait patterns for real-time feedback. We hypothesize that joints proximal to the prosthesis, such as the prosthesis-side hip, will show higher accuracy in joint work estimation due to sensor proximity, while distal joints will be less accurate without sound-side data. We tested three machine learning models on seven subjects with varying sensor datasets. CNN models significantly outperformed TCN models in predicting joint work, with sound-side sensors improving accuracy for distal joints like the sound ankle ( $p < 0.05$ ). Our results confirm that while a minimal sensor set achieves near-optimal accuracy, additional sound-side sensors enhance predictions for distal joints. This study introduces a novel method that reduces reliance on costly motion capture systems, providing a method for real-time feedback for prosthetic optimization and aiding in more balanced and efficient ambulation for amputees.

## **CHAPTER 1: INTRODUCTION AND BACKGROUND**

In the United States alone, the number of amputees has been increasing steadily making the need for prosthetics more crucial [1-3]. To help these individuals restore their ability to walk and continue their day-to-day activities, increased efforts have been made in the development and research of lower-limb prosthetic devices and their capabilities to mimic a biological leg [2-4]. These devices are often categorized into two main types: passive and active. Passive devices generally function as a means of support for the body and are not capable of moving on their own. Their static nature causes users to develop compensatory behaviors in certain activities that often lead to a non-natural range of motion and gait asymmetries [5-7]. Such gait irregular behaviors of bilateral limbs pose certain health risks such as degenerative joint diseases or risks of falling from uneven load distributions [8-10]. In addition, the lack of energy generation at the joints leads to increased metabolic energy expenditure as the user needs to actively move the prosthetic device during ambulation [7,11,12]. Active – also known as powered – prosthetic devices are equipped with onboard sensors and motors to alleviate these issues. They are designed to better emulate the mechanical movement of a biological leg by directly providing powered assistance at the joints as the user ambulates using sensors on board the prosthesis and state-of-the-art control strategies [13-17]. Because of this, powered prostheses can perform a much wider range of tasks than their passive counterpart and can lead to more efficient ambulation by restoring natural gait functionality [18-20].

## **1.1 Sensing on Powered Prosthesis**

There are various ways in which these prosthetic devices are designed and controlled. Common sensor sets include kinematics sensors such as inertial measurement units (IMUs) to detect orientation and acceleration of lower limbs, force sensors or pressure sensors for determining weight distribution and balance of the user, and torque, and position sensors at the joints to measure rotational forces and track angular displacement. Electromyograph (EMG) sensors are also used to attach to the residual muscles of the amputation site to predict the user's intended movements by responding to specific muscle contractions, allowing for more intuitive control [17,21]. Other forms of sensors that are capable of directly sensing the external environment, such as cameras or range sensors, are commonly used as well [22-25]. While there is a wide array of sensors to choose from in designing a prosthetic device, including all these sensors may not always be the most effective design solution. The choice of which sensors to use for a prosthesis and its subsequent control architecture may vary depending on not only the physical limitation of the device itself or the availability of the equipment but also on the specific task at hand. It is important to determine which sensor set holds the minimal necessary information for the prosthesis to provide the user with the most natural movement for efficient and effective ambulation [26,27].

## **1.2 Machine Learning for Prosthesis Control**

The incorporation of data-driven control methods has been a widespread development in the prosthesis domain to enhance the functionality of lower limb prostheses. These sophisticated algorithms have helped in recognizing and learning users'

gait patterns to assist users more efficiently and accurately by adapting to user's movements and intentions [28,29].

One primary use of ML in lower limb prosthetics is for user intent recognition and estimating for locomotion mode. Various works in the past have shown great accuracy in classifying whether the user is in level ground walking, ramp ascent and descent, or stair ascent and descent [16,30,31]. There has been a steady development in such ML algorithms and models, beginning from gradient boosting [32], neural networks (NNs), convolutional neural networks (CNNs) [33], long short-term memory (LSTM) networks [34], and recently temporal convolutional networks (TCNs) [35]. By accurately predicting the user's locomotion mode in real-time, the amount of power actuated at each joint and their respective joint parameters can be adjusted to provide better assistance to the user and improve their overall gait.

Another primary purpose of ML is context estimation by focusing on regression tasks. For example, ML models can be trained to estimate a user's gait speed from prosthesis sensor data [36]. Previous works have compared different models that can achieve this task, and it was shown that ML models in general are capable of outperforming analytical methods that solely rely on kinematic models for computation [36]. Other usages include ground slope estimation and stair height estimation [37]. These models are also trained in estimating for predicting lower-limb joints' kinematics and dynamics as well as in prostheses and exoskeletons by directly predicting for user's joint moments across ambulation modes [38, 39]. Similar to the classification task, these regression estimates can be made in real-time for a better understanding of the prosthesis' live performance as

the user ambulates, which allows for real-time adjustments to further help the user if needed.

### **1.3 Gait Symmetry Measurement**

One of the key goals of lower-limb prostheses is to restore natural gait for the user. Past studies have shown successful results in mode classification and user context estimation for providing better assistance, but their metrics of evaluation are heavily focused on the prosthetic's performance in terms of ML classification accuracy and regression estimate error analysis [30,31]. These results prove that we can reliably predict what the user wants in real time and adjust the amount of assistance provided at each joint to emulate the feeling of a natural gait, but it does not quantify or evaluate the biomechanics of the sound-side limb. To have a better understanding of whether the prosthesis can improve the gait symmetry of the user, there must be a direct evaluation of the performance of the sound limb in real time to compare to the amount of prosthesis assistance.

To evaluate the performance of the lower limb, one metric is to directly measure the joint moments of each leg to evaluate the biomechanical work expenditure. Such has been done widely in exoskeleton assistance, where accurate lower limb joint moment estimation has been capable of predicting real-time joint dynamics for better exoskeleton assistance in various activities [38-40]. Works by Jiang *et al.* and Moghadam *et al.* have done similar analyses, but with smaller sensor sets, such as one or two IMUs at a particular joint to estimate the joint torque at the joint of interest [41,42]. Other methods of evaluation have been in estimating spatial gait parameters, such as step length for gait asymmetry assessment to help restore symmetry in each leg and reduce the metabolic cost of walking

[43]. As such, extensive work has been done with able-bodied individuals with exoskeletons to achieve balance in user gait.

In terms of lower-limb prostheses, the problem becomes a bit more challenging because most often the sensor set being used does not encompass the entire lower limb like in exoskeletons, but rather only the prosthetic leg. In addition, as opposed to able-bodied individuals, those with amputations exhibit larger anomalies in their gaits, and movements are more personalized for each individual depending on the prosthetic device they use daily [44]. This poses a challenge especially for developing robust ML control algorithms as it becomes increasingly difficult to find general patterns across users. There has been some previous work that has focused on improving gait symmetry such as the study done by Feng *et al.* that incorporates a human-in-the-loop optimization for transtibial amputees by directly measuring and comparing ground reaction forces (GRFs) of sound-side and prosthetic-side in real-time [45]. Others have used similar methods through gait mats with force plates to compare the amount of force exhibited on each side [46-48]. When compared to studies done on able-bodied individuals, there is not much in-depth work on analyzing the biomechanics of the sound-side limb in prosthesis users especially in real-time.

#### **1.4 Novelty of Work**

A big challenge in evaluating gait symmetry in real-time is that an external device such as a force plate or gait mat is required to measure and receive feedback on the gait metrics of each leg. Moreover, evaluating biomechanics has mainly been focused on able-bodied individuals, rather than amputees relying on prostheses. This thesis aims to

investigate methods of evaluating lower-limb biomechanics on both the sound and prosthesis sides individually. We are first interested in seeing the plausibility of inter-limb predictions, in which we try to estimate the biomechanics of the sound-side limb with only onboard sensors on the prosthesis. Being able to predict the sound limb joint kinematics would be a great measure for analytically evaluating how well the prosthesis is assisting the user by looking at the user's joint work on the sound leg with varying prosthesis joint parameters. We then investigate the most optimal/minimal set of sensors that are required for reliable sound-side limb predictions and compare different types of machine-learning models that are suitable for the task. While this thesis mainly focuses on level ground walking, to explore the robustness of these models and examine how well it translate over to various other modes of ambulation, we also do a preliminary study on ramp walking.

It is hypothesized that inter-limb joint work predictions using only prosthetic sensors will show statistically significant differences in accuracy compared to predictions that incorporate data from the sound-side limb. Predictions for joints closer to the prosthetic limb, such as the prosthesis-side hip, are expected to be more accurate due to the proximity of the sensors, which allows ML models to capture data trends more effectively. In contrast, predictions for joints further away from the prosthetic limb are anticipated to be less accurate without the additional data from sensors on the sound-side limb. When estimating for joint power of each joint, certain joints may be easier to estimate than others depending on how dynamic their movements are. To find the optimal set of additional sound-side sensors, we aim to identify a smaller subset of sensors that can provide accurate joint work estimation. Although a full set of sensors on the sound limb would theoretically yield the best work estimations due to the richer dataset, our goal is to achieve similar levels of

accuracy with a minimally invasive set of sensors. This approach would augment prosthesis-only sensing and enhance the practicality and comfort for the user.

## CHAPTER 2: OPEN SOURCE LEG

This chapter provides an overview of the powered knee-ankle prosthesis, Open-Source Leg (OSL) developed by the University of Michigan [49], used for this thesis. The first section of this chapter describes the various sensors and actuators on the device that are used to control and receive feedback on the leg. The next section examines the three-level hierarchical architecture of the controller utilized by the device.

### 2.1 Onboard Sensors and Actuators

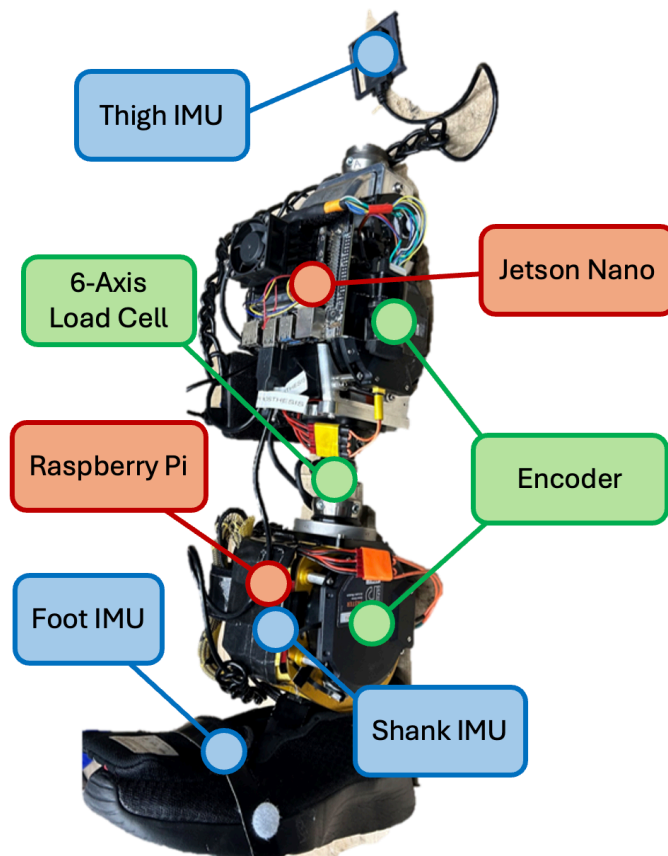


Figure 1. Open-Source Leg (OSL) onboard sensors.

The OSL seen in Figure 1 is a knee-ankle prosthesis, meaning there are two actuated joints capable of providing positive power and movement in the sagittal plane, one at the knee and another at the ankle, and are intended to be used for transfemoral (TF) amputees. There is an encoder at each joint used to calculate joint angular kinematics and a single six-degree-of-freedom load cell between the two joints to measure the force experienced through the device as the user ambulates. In addition, there are three six-degree IMUs, one at each body segment (thigh, shank, foot). This equates to a total of 28 sensor signals recorded by the prosthesis. All real-time processing occurs on a mounted Raspberry Pi and NVIDIA Jetson Nano microcontroller, which are responsible for taking sensor data to run ML algorithms and command appropriate control signals to the joint motors. Physically, the knee range of motion ranges from  $0^\circ$  to  $120^\circ$ , while the ankle ranges from  $20^\circ$  dorsiflexion to  $10^\circ$  plantarflexion. The control system (Figure 2) of the leg is divided into three different levels: high, medium, and low, which will be discussed further in the following section.

## **2.2 Controller Design**

### *2.2.1 High-level controller*

The high-level controller houses the ML algorithms that are responsible for mode classification tasks to detect user intention and make context estimations for regression tasks such as walking speed or slope angle estimations. These ML models are pre-trained and run in real-time on the Jetson Nano and Raspberry Pi.

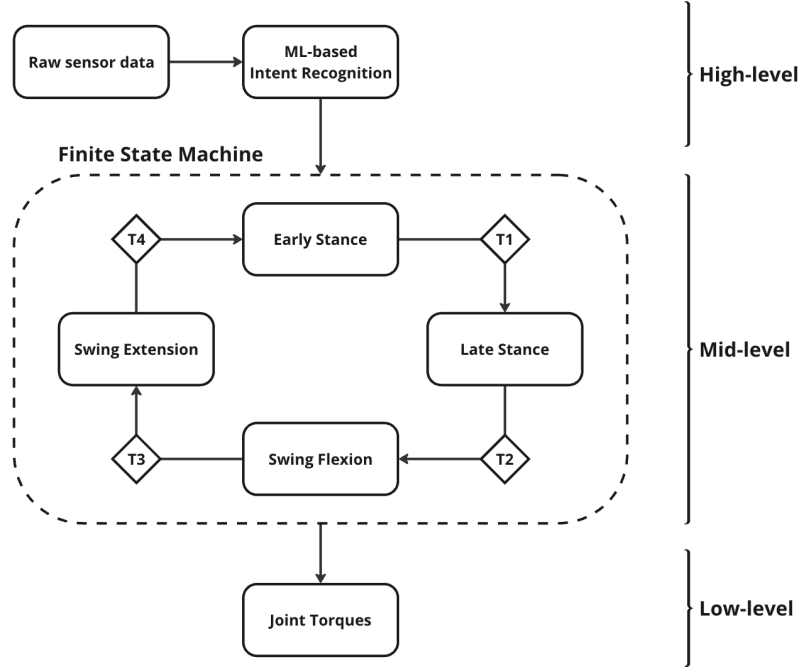


**Figure 2. OSL hierarchical control structure.**

### 2.2.2 Mid-level controller

At the mid-level controller, the mode predictions from the high-level controller are passed down to determine the appropriate torque required at each joint depending on the specific gait mode and phases. The OSL uses a finite-state machine (FSM) based controller along with impedance parameters to provide an intuitive gait phase model [50]. The desired, or commanded, impedance torque values  $\tau$  are governed by the equation:

$$\tau = -k(\theta - \theta_{eq}) - b\dot{\theta} \quad (1)$$

For each respective joint,  $\theta$ ,  $\theta_{eq}$ , and  $\dot{\theta}$  represent the current angle, target angle, and angular velocity, while  $k$  and  $b$  are the stiffness and damping coefficients. The FSM

is defined by five different ambulation modes: level walking, ramp ascent, ramp descent, stair ascent, and stair descent. Each mode is further separated into four different gait phases and four transitions between the phases. The phases are defined with two stance phases, early stance, and late stance, and two swing phases, swing flexion and swing extension. These transitions between phases are triggered through certain conditions, such as ankle angle threshold between early to late stance, vertical load threshold between late stance to swing flexion and swing extension to early stance, and knee angular velocity threshold between swing flexion and extension. On top of this, various bio-inspired control strategies and parameter shaping equations proposed by Simon *et al.* are implemented based on the impedance and joint parameters to provide the user with more natural ambulation in various modes [51].

### 2.2.3 *Low-level controller*

At the low level, the desired torque values from the mid-level controller are passed onto the actuators with a built-in PID controller to provide the desired scaled assistance to the joints.

## CHAPTER 3: METHODOLOGY AND MACHINE LEARNING

### MODEL DESIGN

#### 3.1 Experiment Protocol

This study was conducted in the Exoskeleton and Prosthesis Intelligent Controls Lab's terrain park located in Georgia Tech's Callaway Manufacturing Research Center building, as shown in Figure 3. The terrain park is equipped with VICON Motion Capture system, which allows for capturing the biomechanical information of a subject equipped with reflective markers at various points along the body.

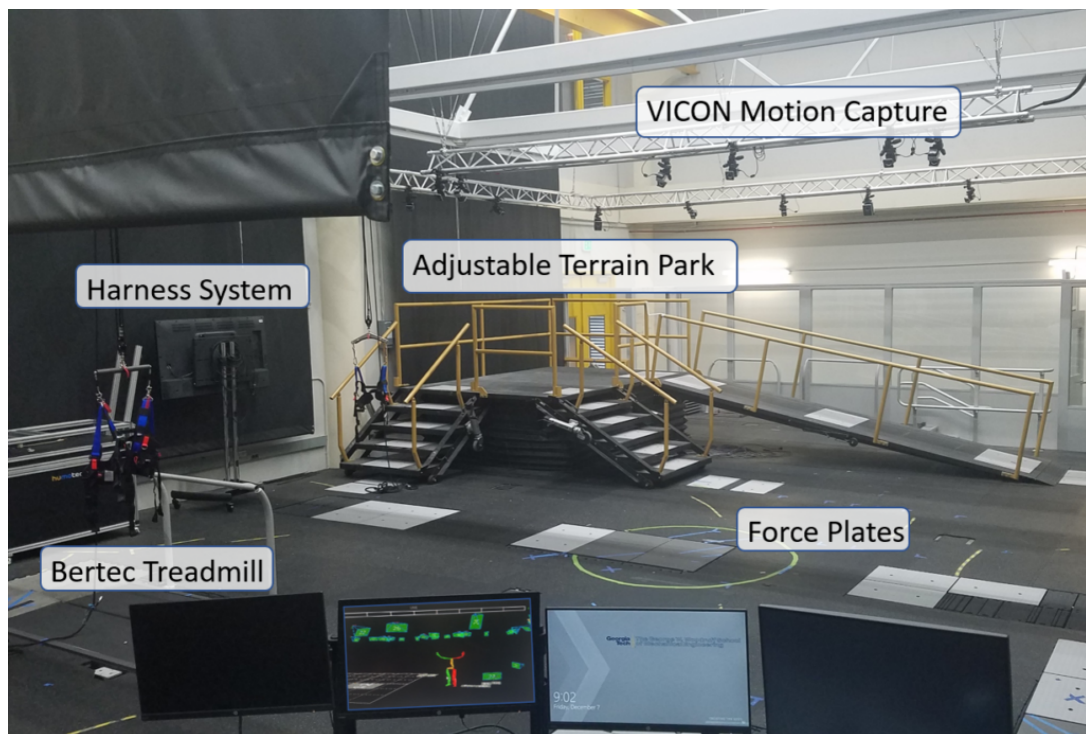


**Figure 3. Terrain park used for various experimental protocols. VICON system allows for motion-capturing capabilities and force plates make it possible to calculate ground reaction forces as the user ambulates around the park.**

The main experiment consisted of seven individuals with unilateral transfemoral amputation (N=7, encoded with the TF subject number, age:  $39.5 \pm 14.5$ , mass:  $70.5 \pm 8.2$  kg, height:  $168.5 \pm 9.7$  cm). Most subjects rely on a passive prosthesis for daily use, but some use commercially available prostheses such as the Rheo Knee developed by Ossur. During the beginning of the session, subjects were fitted by a prosthetist with the active OSL and were required to complete a training and tuning session to ensure proper impedance parameters for the user's comfort. Subjects were then instructed to walk on the Bertec dual belt treadmill with built-in Bertec Force Plates. During the data collection session, the subjects walked on the level treadmill for five minutes, during which the speed of the treadmill was varied dynamically between 0.3 m/s to 0.9 m/s throughout the trial. A total of 12 trials were collected for each subject.

The second experiment consisted of another seven sets of individuals with unilateral transfemoral amputation (N=7, same TF encoding with subject number, age:  $42 \pm 12.4$ , mass:  $84.7 \pm 15.7$  kg, height:  $173.5 \pm 9.4$  cm). Between the two experiments, three subjects participated in both sessions. Similar to the first experiment, the subjects were appropriately fitted and trained on the OSL before the session, and they were instructed to walk up and down the ramp of the adjustable terrain park for a total of five trials at four slope angle conditions:  $7.8^\circ$ ,  $9.2^\circ$ ,  $10.8^\circ$ , and  $12.4^\circ$ . Four Bertec Force Plates were placed at around the halfway point of the ramp, and the subjects were instructed to ensure that the entire foot was in contact with the force plate when walking over them to record proper GRF sensing. Before performing either of the two experimental protocols, a static pose of each subject was recorded for accurate model scaling in the biomechanics reconstruction process.

### 3.1.1 Biomechanics Processing

The VICON motion capture data was first labeled within VICON software to identify trajectories for each body marker. Any gaps in the marker trajectories were filled (rigid body and pattern fill) using an automated pipeline and processed through OpenSim [52] with a modified standard lower limb model (Simbody gait2392) adapted for the OSL [53] to calculate inverse kinematics and dynamics. An example of the OpenSim musculoskeletal model of a subject can be seen in Figure 4.

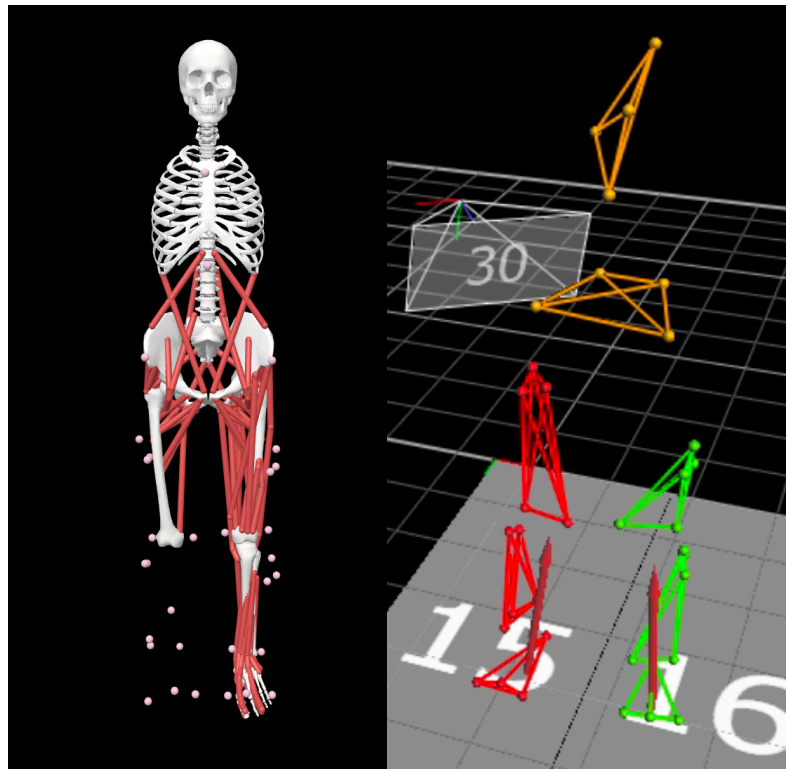


**Figure 4. Musculoskeletal model of a subject in OpenSim on left and motion capture makers in VICON software on right.**

In terms of the marker set used, there were a total of four upper body markers, four pelvis markers, three thigh markers for each side, three shank markers for intact limb, two

markers at the knee joint and intact ankle, four foot markers, and nine OSL markers. First, a scaled model of the subject is generated, and inverse kinematics and inverse dynamics are computed with the scaled model with OpenSim's built-in Inverse Kinematics and Inverse Dynamics tools. To calculate the joint moment, the angular velocity of each joint was multiplied by the individual torques, and the derived power curve can be integrated over time to get the joint energy for a specified time duration. The joint moments were also normalized for each subject's body mass.

In terms of data frequency, the raw motion capture data was recorded at 200 Hz, resulting in the inverse kinematics and dynamics also being at 200 Hz, while the Bertec force plates recorded the GRFs at 1000 Hz. The motion capture data was lowpass filtered using a zero-lag, Butterworth filter with a 6 Hz cutoff frequency, and the GRFs were filtered with a 20 Hz cutoff frequency. Because the onboard sensors on the OSL were collected at a lower frequency of around 100 Hz, all biomechanical data was downsampled and time-synced to match with the prosthesis sensors.

### *3.1.2 Sound-side Sensor Simulation*

Due to experimental limitations, data was collected without any sensors on the sound side, so sensors were synthesized on the sound side using VICON marker trajectories of the sound limb and OpenSim, using methods inspired by Molinaro *et al.* [40,54]. Particularly, three IMUs were simulated at each of the intact limbs: femur, tibia, and foot. Each IMU had six channels of data, three degrees of linear acceleration, and three degrees of angular velocity. We also simulated an insole sensor at the foot by translating and rotating the GRFs to the foot frame and calculating the mediolateral and anterior-posterior

center of pressure (CoP), providing a total of three data channels (Figure 5). In summary, there were three main simulated sensors on the sound-side: two IMUs with six features each, and a foot insole with an IMU and vertical force sensing.

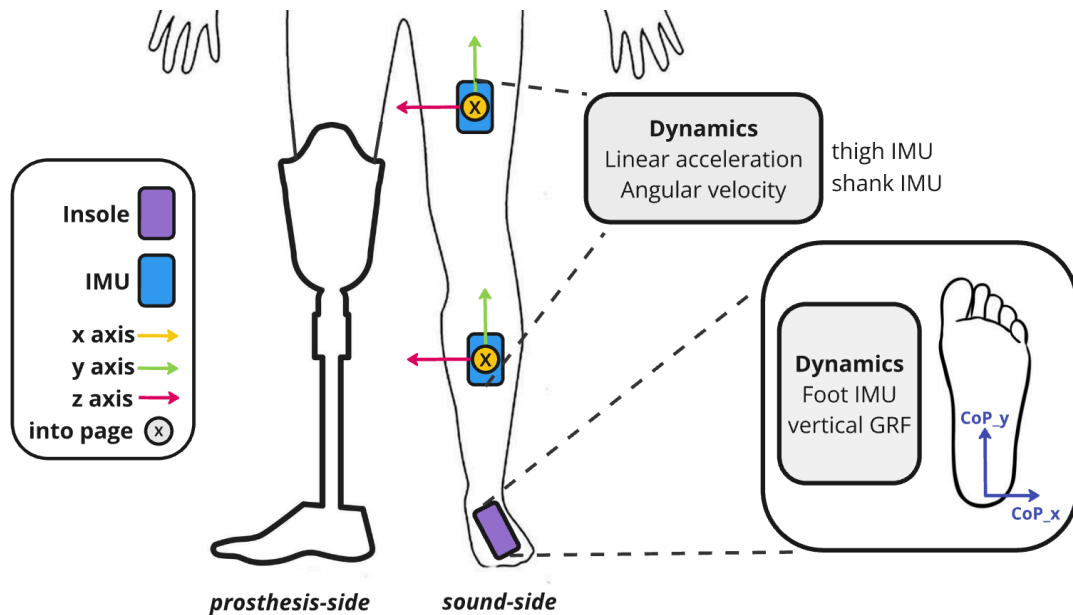


**Figure 5. Simulated IMU and foot insole location and axes.**

### 3.1.3 Data Pre-processing for Machine Learning

For the data to be used for the ML models, various steps of data pre-processing were required. While certain models can work with raw sensor data without any modulations, others, especially those that depend on kernels or windows of data to obtain temporal information, need the data to be formatted in specific ways.

The first step taken was cleaning up and reformatting the data for proper training of the models. Because joint work is an integrated metric that needs an accumulation of data, the entire dataset must be divided into separate segments. For the most logical

analysis, we decided to train and test the ML models in a stride-by-stride fashion. As a result, for each level walking trial, the timestamp of each heel-strike was calculated by setting a threshold vertical GRFs value, and every heel-strike to heel-strike was defined as a full gait cycle. Each cycle was saved as a Python Pandas DataFrame object for easier retrieval. For the ramp dataset, the data-cleaning process was similar. However, unlike the walking trials in which at least one of the subject's feet is in contact with a force plate, ramp trials have GRF data only around the four force plates placed on the terrain park. It is important to segment the data out to where GRF are recorded because that is the only way of computing valid inverse dynamics from biomechanical analysis. As a result, while walking trials consist of an ample amount of step data, ramp trials for each subject only consist of four to five valid steps for each trial. This may lead to potential issues when training and testing the ML models which will be discussed further in the later sections.

## **3.2 Machine Learning Models**

As aforementioned, ML techniques have been a great method of reliably helping predict user intent recognition and context estimation in lower limb prostheses. From a wide array of models to choose from, this thesis explores two different algorithms: the CNN and the TCN.

### *3.2.1 Convolutional Neural Network (CNN)*

A CNN is a specialized type of artificial NN that is mainly designed to process and analyze two-dimensional data, particularly visual data, making it effective for tasks such as image recognition, classification, and segmentation. However, there has been growing use of CNNs in one-dimension with time-series data due to their ability to automatically

extract and learn features, which makes it highly beneficial for analyzing temporal patterns (Figure 6). When compared to other deep learning architectures such as LSTMs or gradient boosting algorithms such as XGBoost, CNNs have shown to be more accurate and computationally more efficient when it comes to various tasks associated with wearable devices [29,42].

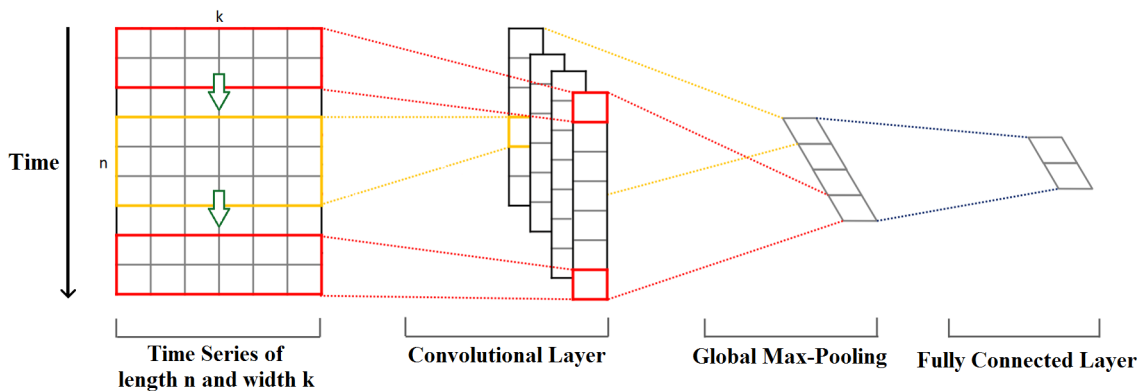


**Figure 6. Overview of a CNN architecture and data transformation [57].**

In the context of time-series data, within the 1-D convolutional layer filters or kernels of a specified size slide over the time axis, capturing local temporal patterns. These weighted filters essentially generate a feature map at each layer to highlight the important patterns and trends within the data. This automated feature extraction and temporal awareness is a key advantage of a CNN, as other methods such as XGBoost rely on a manual feature extraction process and are not able to capture temporal relationships between subsequent time-series data.

CNNs also consist of pooling layers that are used to reduce the dimensionality of the constructed feature maps. By down-sampling the data, the model reduces the computational load and makes the network more robust to variations in the input. A typical CNN architecture consists of a hierarchical learning process, in which multiple convolutional layers are stacked to start by learning low-level patterns in the early layers to more complex patterns in the deeper layers. Such structure is crucial when capturing temporal dependencies and structures within time-series data.

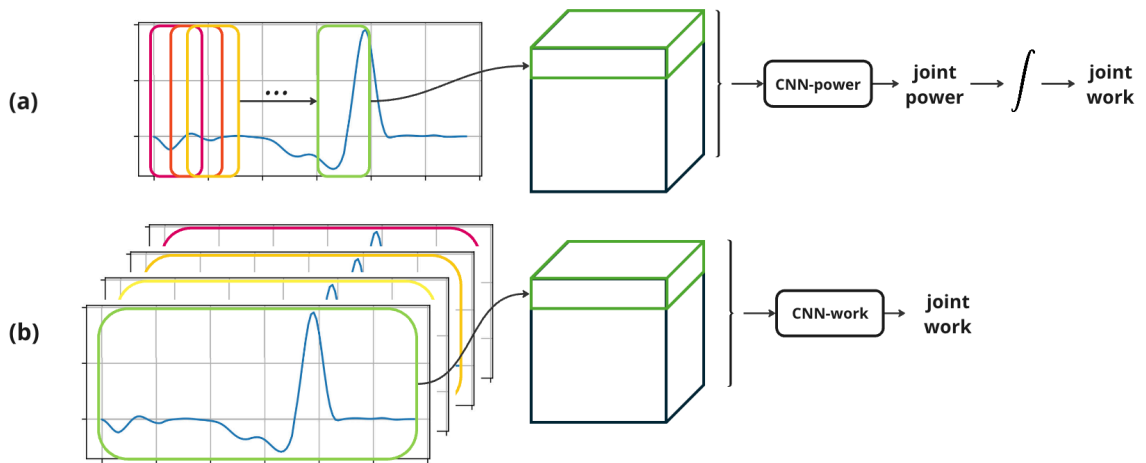


**Figure 7. (a) CNN for joint power estimation (b) CNN for joint work estimation.**

In this thesis, two different models of CNNs are explored as seen in Figure 7: CNN for joint power estimation and CNN for direct joint work estimation. The first model is trained with the joint power as the label, and the resulting predicted power curve is integrated over a gait cycle to calculate the joint work. The latter model is trained on each gait cycle with one overall work value as the label per cycle. We explore whether there is

a significant difference in the two estimation methods, and which might have an advantage over the other. The exact architecture of the two models is discussed in a later section.

### 3.2.2 Temporal Convolutional Network (TCN)

A TCN, introduced by Bai *et al.* [35], is a NN model that is specifically designed for sequence modelling tasks. TCNs leverage the principles of CNNs, but they explicitly leverage the temporal information in the input data. On top of the causal convolution that is formed from the convolutional layers similar to a CNN, the TCN introduces the concept of dilation as well. The use of a dilated 1-D convolution (Figure 8) allows for an increased receptive field of the model without increasing the number of parameters or the computational cost significantly. Compared to a standard convolution, the kernel elements are spaced out by a certain dilation factor, and by exponentially increasing the dilation factor through stacked convolutional layers, we can effectively capture patterns over longer periods by seeing more data points at once as seen in Figure X.

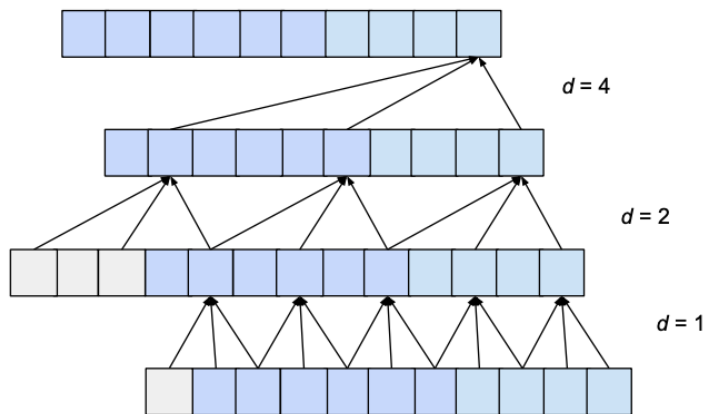


**Figure 8. Convolutional dilation in a TCN [56].**

These convolutional layers are organized into what are known as residual blocks seen in Figure 9, where the input to a block is passed through the convolutional layers, and their outputs are added to the original input. This residual connection allows for the layers within the residual block to learn to model the difference between the input and the desired output, making it easier for the network to learn identity mapping and ensure deeper layers do not degrade the performance of the network. Overall, this helps in improving gradient flow and stabilizing the training process of the model.

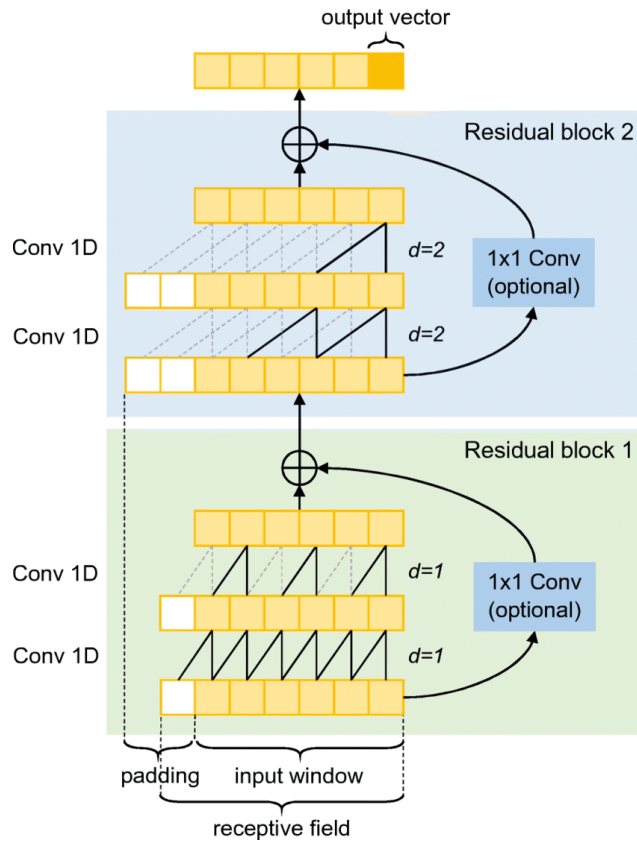


**Figure 9. Residual block connection in a TCN [55].**

### 3.2.3 Model Hyperparameter Optimization and Training

To determine the most optimal model architecture for the ML models, the parameters of the models were optimized through a hyperparameter sweep. For the CNN models, a grid search was utilized to sweep through a set of candidate values for each hyperparameter, which can be seen in Table 1. The optimization process was done through two steps: first, the layers of the model were optimized, then the parameters for each of the layers were determined. The TCN hyperparameters seen in Table 2 were selected based on a previous optimization done by Scherpereel *et al.* based on the architecture by Molinaro *et al.* [40] whose work focused on improving biological joint moment estimation during real-world tasks using EMG and instrumented insoles [39].

**Table 1. CNN hyperparameters and training.**

Hyperparameter	Candidate values	Selected values
# of conv. layers	1, 2, 3, 4	2
# of dense layers	1, 2, 3, 4	2
# of filters each layer	16, 32, 64, 128	(32, 64)
# of units in dense layer	10, 25, 50, 100	(50, 25)
Kernel size	3, 5, 10	5
Pool size	3, 5, 10	5
Dropout	0, 0.1, 0.2, 0.3, 0.4, 0.5	0.3
Learning rate	1e-5, 3e-5, 5e-5, 1e-4	5e-5
Window size	30, 40, 50, 60, 70, 80, 90, 100	50
Batch size	16, 32, 64	32

**Table 2. TCN hyperparameters**

Hyperparameter	Selected values
# of filters	80
# of levels	5
Kernel size	5
Activation function	ReLU
Learning rate	5e-5
Spatial dropout	0.15

For the training of the model, the Adam optimizer was used along with a mean squared error (MSE) loss function. Each of the models was run to a maximum of 200 epochs, with an early stopping criterion for terminating training if no improvements were seen in the validation loss for five consecutive epochs to prevent model overfitting. All models were trained in a user-independent fashion, meaning the training set did not include any of the tested subject's data, and a 7-fold leave one-subject-out validation method was used. The CNNs were based on TensorFlow, while the TCNs were implemented on PyTorch.

### 3.2.4 Joint Work Analysis

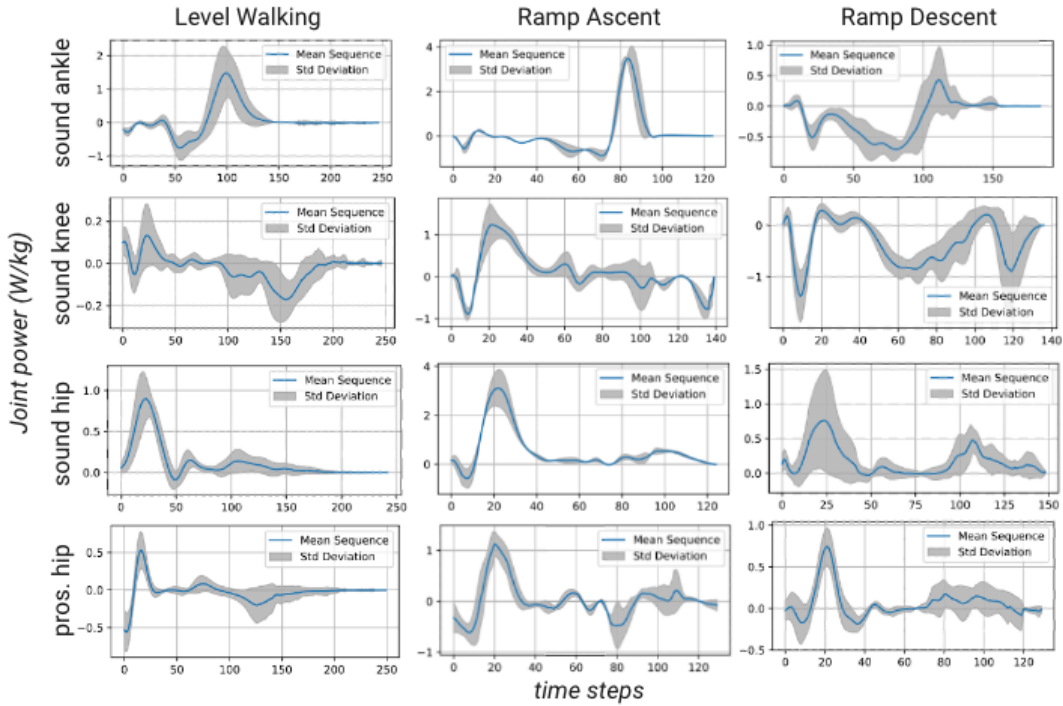


**Figure 10. Visualization of the joint power curves of each of the intact joints for different locomotion modes. The plots show averaged joint power over all collected gait cycles for one random subject and the associated standard deviation. The same subject is shown across all modes and joints.**

In analyzing the joint work for the different locomotion modes, we decide to focus only on the positive work values for level walking and ramp ascent. The predominance of positive joint work during level walking and ramp ascent compared to negative joint work is due to the need for propulsion and elevation [58]. During these activities, muscles like the ankle plantar flexors and hip extensors generate significant positive work (Figure 10) to propel the body forward and lift it against gravity [58]. This involves concentric muscle contractions, where muscles shorten while generating force, and the efficient transfer and

storage of elastic energy. Negative work, associated with energy absorption and deceleration, is less dominant as the primary goal is to generate forward and upward movement, making positive work essential for efficient locomotion. On the other hand, during ramp descent, there is comparatively more negative joint work due to the need for controlled deceleration and shock absorption. Muscles such as the quadriceps and ankle dorsiflexors perform eccentric contractions, where they lengthen while generating force to control the downward motion and prevent uncontrolled falling [58]. This negative work helps manage the body's descent by absorbing energy and reducing impact forces on the joints. Therefore, the primary goal during ramp descent is to decelerate and stabilize the body, resulting in increased negative work compared to positive work. Therefore, we only analyze the negative work in ramp descent. Such biomechanic trends are observed thoroughly within able-bodied individuals [59].

### *3.2.5 Work Correlation Coefficient Analysis*

The primary metric of evaluation for all results is the R correlation coefficient between predicted and ground-truth work for a given data window. In the case of power-based models, the work for each window of data was based on the architecture of the ML model (window size). For the work-based model, the window size spanned a full gait cycle, heel-strike to heel-strike. For each subject the model was tested on, an average R-value of all gait cycles was computed and compared across subjects to find an overall mean R for each given model and sensor configuration. Evaluating the correlation between the predicted and actual work is a better metric than a quantitative measure such as mean absolute error or mean squared error because we are mainly interested in whether the ML models are capable of qualitatively recognizing the sound-side kinematic changes that

occur as the user walks at various speeds. A qualitative measure is sufficient in future applications of control optimization as will be discussed in the later sections.

### 3.2.6 *Statistical Analysis*

We conducted a one-way repeated measures analysis of variance (ANOVA) with an alpha level of 0.05 to compare the performance of each ML model across all joints. For each joint analysis, model and subject were defined as independent variables, and predicted vs actual work correlation coefficient (R-value) was the dependent variable. Bonferroni post-hoc tests were used to make pairwise comparisons to understand if there were statistical differences between each individual condition for each analysis. When doing sensor configuration analysis to compare the different sound-side sensor subsets, because we have seven different configurations, which require too many statistical comparisons, we mainly compare each configuration to the result of all sound-side sensors. This is because we are under the assumption that all sensors yield the best joint work estimations. For each pairwise test, we do a simple t-test with an alpha level of 0.05 for each joint. The independent variable is the sensor configuration and the R-value is the dependent variable for each joint, with subject being random. When comparing the multi-modal model across level walking and ramp trials, because there were only three overlapping subjects between the two experiments with a total of N=11 subjects, an ANOVA test cannot be used for statistical analysis due to unbalanced data across modes (i.e. LW vs. RA or LW vs. RD). Thus, we conducted a linear mixed model analysis with an alpha level of 0.05. The R-value was the dependent variable, random effects for subjects to account were included for within-subject variability, and Bonferroni post-hoc tests for pairwise comparisons.

## **CHAPTER 4: RESULTS**

This chapter will present the results of data collection, processing, and the performance of the various ML models in different sensor configurations and ambulation modes. The first section will focus on comparing the ML models in level-ground walking across subjects and explore the viability of inter-joint work estimations using prosthesis sensors. The second section will cover results on sound-side sensor optimization to determine the optimal minimal set of sound-side sensors for estimating joint work in prosthesis users. Finally, the last section will show a preliminary expansion into conducting similar analyses on user ramp data.

## 4.1 Inter-Joint Estimation Model Comparison

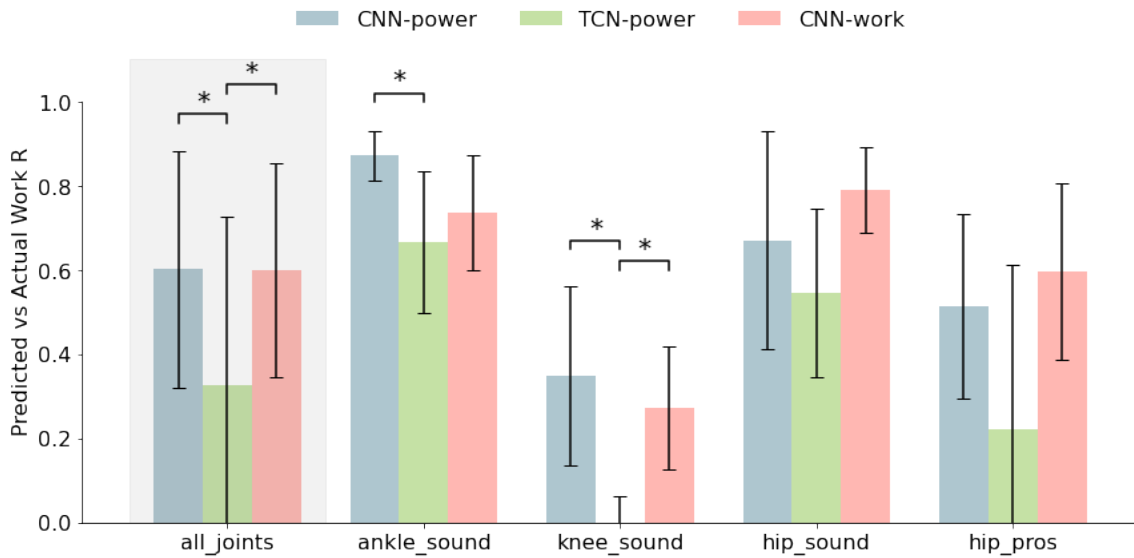


**Figure 11. Comparison of ML models’ performances in estimating each of the joint work. Sound joints are trained and estimated using full sound-side sensors, while prosthesis joints use only prosthesis sensors. Error bars represent  $\pm 1$  standard deviation across all subjects and asterisks indicate statistical significance ( $p < 0.05$ ).**

When comparing the models’ performances by examining their predictions on all the joints combined in Figure 11, both CNN methods are seen to outperform the TCN method by a significant margin ( $p < 0.05$ ). Between the CNN models, there are no statistically significant ( $p < 0.05$ ) differences between the direct work estimation and joint moment curve integration methods across the different joints.

The differences in results are more evident when examining each joint individually. Overall, the sound-side ankle and hip joints yielded the best estimations across all models, while the prosthesis-side hip joint had an average performance. The sound-side knee seemed to be a difficult task in general, but the two CNN methods were able to detect weak

to moderate levels of correlation ( $0.35 \pm 0.21$  and  $0.27 \pm 0.15$ ). The general performance of the models across the joints follows the same trend as the results from all the joints combined, where the CNNs appear to produce better estimations than the TCN. As a result, moving forward, we focus primarily on these two models and examine in detail how varying input data affects their performances.

#### 4.1.1 CNN Power to Work Integration Model

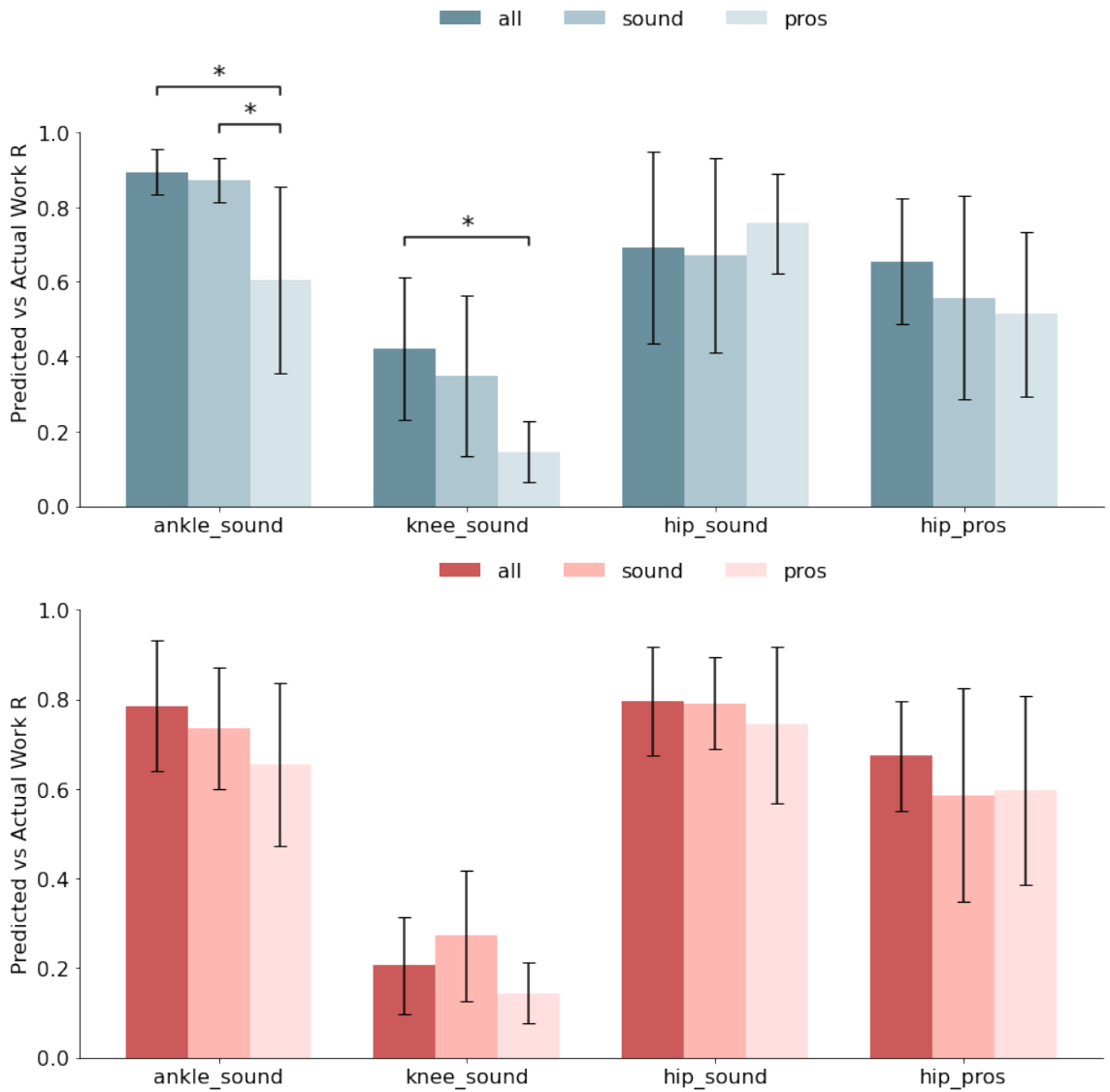


**Figure 12. Sensor variation on each joint work estimation in level walking using CNN-power model (above) and CNN-work model (below). Error bars represent  $\pm 1$  standard deviation across all subjects (N=7) and asterisks indicate statistical significance ( $p < 0.05$ ).**

For the CNN-power model, the sound ankle and knee joints showed statistically significant ( $p < 0.05$ ) differences between the sensor configurations. No statistical

differences ( $p > 0.05$ ) were observed across sensor sets for the hip joint estimations bilaterally. Similar to the findings from the previous section, the average joint estimations rank from highest to lowest as ankle, knee, then hip. For the CNN-work model, there were no significant differences ( $p > 0.05$ ) when adding sound-side sensors to the prosthesis side in terms of joint work estimations for all the joints. Qualitatively, higher joint work correlation values in the hip are observed with the direct work method compared to the power to work integration method.

#### **4.2 Sound-Side Sensor-Set Optimization**

While it is hypothesized that using a full array of sound-side sensors will give the most accurate measure for sound-limb gait characteristics, it is often not ideal to add additional sensors for the user for the sake of user comfort and efficiency. For prosthesis users especially, apart from the prosthesis itself, we want to avoid adding additional sensors for the user to wear. Given that having direct sound-side sensing is optimal for estimating sound-side joint metrics, as discussed in section 4.1, we want to investigate the minimal set of sensor sets required to get robust and accurate estimations.

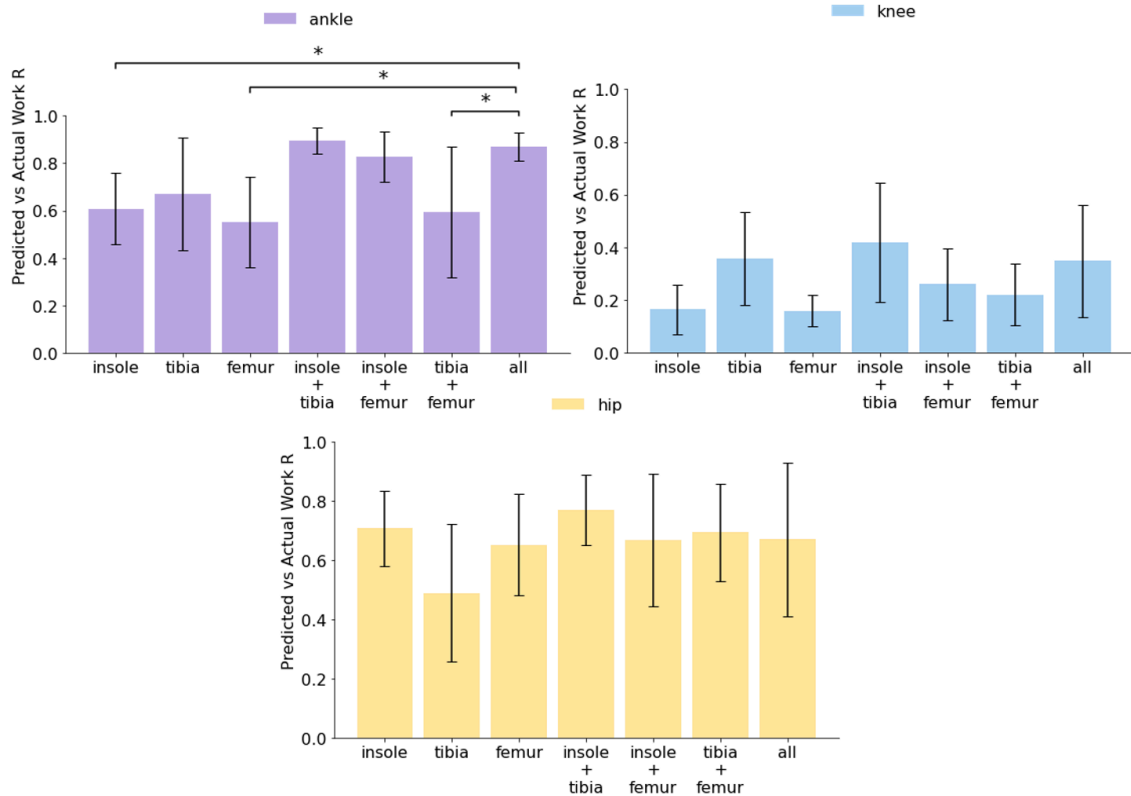


**Figure 13. Sound-side sensor subset comparison using the CNN-power model on sound-side joints. Error bars represent  $\pm 1$  standard deviation across all subjects (N=7) and asterisks indicate statistical significance ( $p < 0.05$ ).**

There is no statistical significance ( $p > 0.05$ ) in the performance of the model across various sensor configurations on the sound-side apart from the ankle joint, where having all sensors and using just the insole and tibia IMU was significantly better than the case of using only the femur IMU. The best results were obtained with a combination of two sensors, specifically the foot insole with either the tibia or femur IMU. For the knee joint, the best correlations were observed with the insole and tibia combination, while the tibia performed best as a single sensor. However, sensor configuration did not significantly affect the knee joint, and overall accuracy was moderate. For the hip joint, the tibia was

the least accurate single sensor, while the insole was the best, followed by the femur. The accuracy for the hip joint was relatively strong across all sensors, with single sensors (insole or femur IMU) providing similar accuracy to the full sensor set. Overall, the insole and tibia combination emerged as the best sensor set for all three sound joints.

### **4.3 Multi-Modal Estimation**

To test the robustness of the models and how they can perform in other ambulation modes, the same analysis is done with users walking up and down a ramp at various incline angles. Because the ramp dataset was significantly smaller than that of the level walking data due to the setup of the terrain park, where only a few steps were captured over the Bertec force plates during ramp trials, only the CNN-power model was explored. To see how well the model generalizes to new modes, we use the same models from the previous sections trained on level walking data and train it further with additional ramp data.

### 4.3.1 Combined LW and Ramps CNN

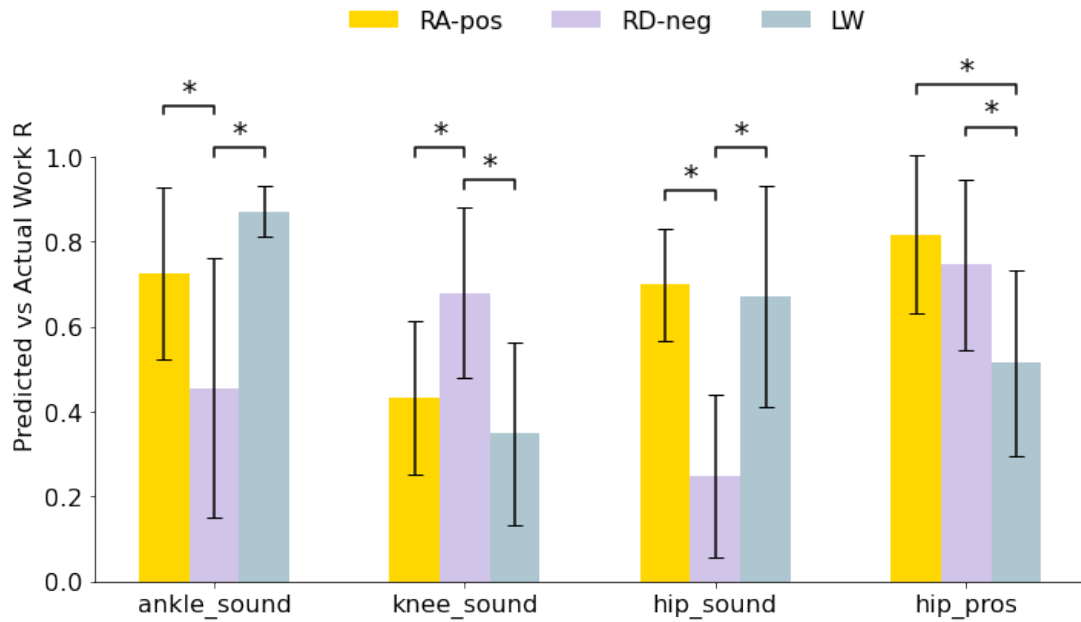


**Figure 14. Combined LW and ramps CNN-power model for estimating each of the joint works. Sound joints are trained and estimated using full sound-side sensors, while prosthesis joints use only prosthesis sensors. Error bars represent  $\pm 1$  standard deviation across all subjects ( $N=7$  for ramps and  $N=7$  for level walking) and asterisks indicate statistical significance ( $p < 0.05$ ).**

The performance of the CNN-power model has a significant difference ( $p < 0.05$ ) between LW and RD-neg for all joints. Similar comparisons are also seen between RA-pos and RD-neg, except for the residual side hip, where the model estimated equally for the two modes ( $p > 0.05$ ). Apart from the prosthesis-side hip joint, there are no statistically significant differences between RA-pos and LW in joint work correlation. The model appears to perform well with estimating positive work during ramp ascent for all joints apart from the sound knee. During ramp descent where the negative work becomes more

significant, the model predictions have a high correlation with the sound knee ( $0.68 \pm 0.20$ ) and prosthetic-side hip ( $0.75 \pm 0.20$ ).

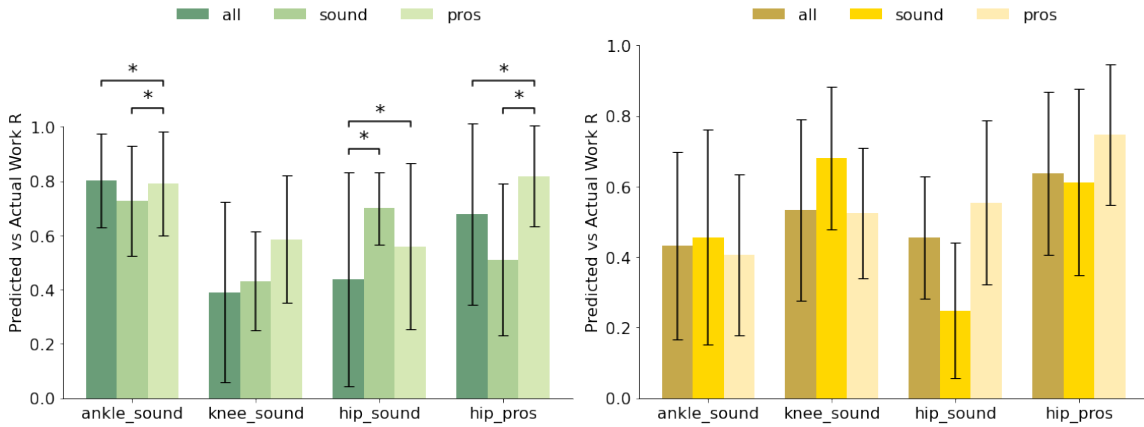


**Figure 15. Inter-limb joint power estimation in ramp ascent positive work (left) and ramp descent negative work (right) correlations. The CNN-power model trained on both level walking and ramp trials. Error bars represent  $\pm 1$  standard deviation across all subjects (N=7) and asterisks indicate statistical significance ( $p < 0.05$ ).**

Once again, we are interested in inter-joint estimations during ramp trials as well. In ramp ascent, the sound ankle saw statistically significant ( $p < 0.05$ ) differences across the sensor sets, with the full sensing yielding the highest work correlation ( $0.80 \pm 0.17$ ). Work estimations are seen to decrease with the addition of sound-side sensors to prosthesis sensors in the hip joints. There are no significant differences ( $p > 0.05$ ) between the sensor sets for the knee joint. Compared to the level walking results from the previous sections, same-side correlations (prosthesis sensors for prosthesis hip and sound sensors for sound joints) appear to be better during ramps, especially with the prosthesis-side hip. Similarly, in ramp descent, no statistically significant differences were found across the sensor sets for all the joints. The most significant improvement is in the sound knee joint where all sensor configurations can capture moderate levels of correlation compared to the results

from other modes. In general, ramp descent has more variability in the estimated work values.

#### *4.3.2 Sound-side sensor sweep for ramps*

To determine the most minimal sensor set for same-side sensing for the sound limb, a full sweep of sensor sets is conducted on the ramp models as well. The following Figures 16 through 18 are separated by each of the individual joints. The model used was the combined LW and ramp model. For the ankle joint as seen in Figure 16, the best sensor combination is calculated as the tibia and femur IMUs together for ramp ascent. Individually, the tibia IMU appears to be the most useful, and its correlation values are comparable to the best combination and the full sensor set. In general, the model tends to have better estimations for ramp ascent than descent. The R values are quite consistent for ramp descent negative work specifically, with no statistically significant differences seen across the sensor configuration for both ramp ascent and descent.

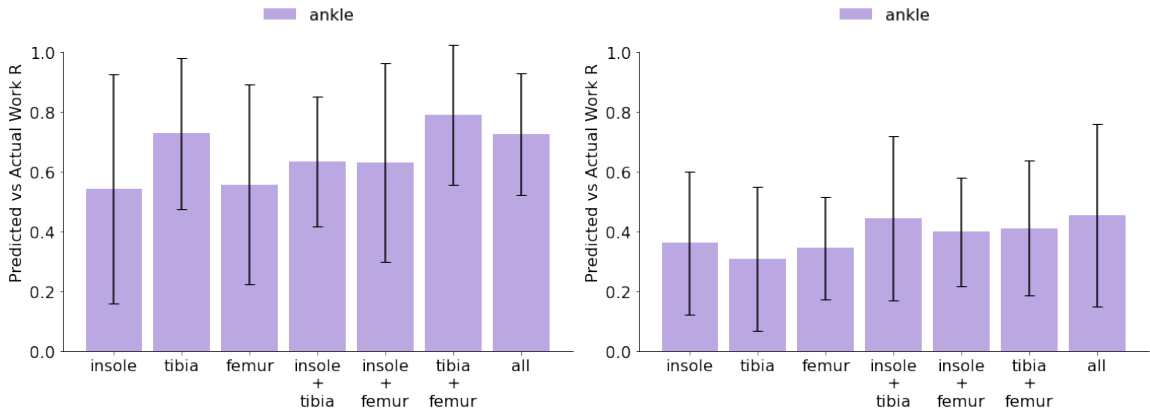


**Figure 16. Sound-side sensor subset comparison using a level-walking and ramp trained CNN-power model on sound-side ankle joint during ramp ascent (left) and ramp descent (right). Error bars represent  $\pm 1$  standard deviation across all subjects (N=7).**

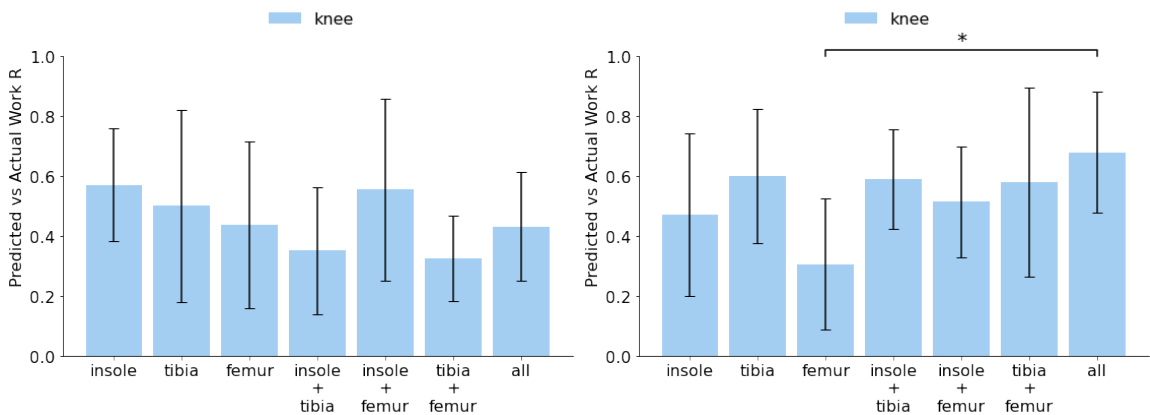


**Figure 17. Sound-side sensor subset comparison using a level-walking and ramp trained CNN-power model on the sound-side knee joint during ramp ascent (left) and ramp descent (right). Error bars represent  $\pm 1$  standard deviation across all subjects (N=7).**

For the knee in ramp ascent, no significant differences ( $p < 0.05$ ) is found across the configurations. Qualitatively, using a single sensor has better estimations compared to their multi-sensor counterparts. For example, having just the insole yields the highest correlation

for ramp ascent. Adding additional sensors seems to decrease the accuracy of the prediction as well, and using all sensors does not yield the best joint estimations. For ramp descent, a significant difference ( $p < 0.05$ ) is seen between all sensors vs. just the femur IMU. General trends show having all the sensors on the sound-side has the highest correlation estimation, although no other statistically significant differences are found. For the hip joint, we see a statistically significant difference between the insole and all sensors in both ramp ascent and descent. While all sensors give a higher joint estimation in ascent, it is the worst during descent. Best sensor set appears to be either all the sensors combined of the insole and tibia together for ascent, like that of level walking.

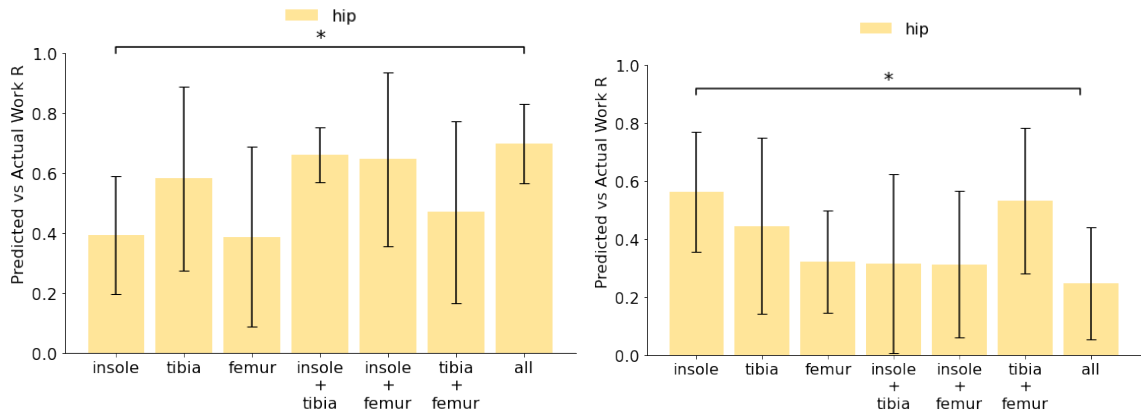


**Figure 18. Sound-side sensor subset comparison using a level-walking and ramp trained CNN-power model on the sound-side hip joint during ramp ascent (left) and ramp descent (right). Error bars represent  $\pm 1$  standard deviation across all subjects.**

## CHAPTER 5: DISCUSSION

This study presents a way to estimate sound-side limb joint work for prosthesis users without potentially needing extra sensors on the sound leg. The main hypothesis was that inter-limb joint work estimations using only prosthesis sensors would have significantly lower joint work correlation values than when using additional sound-side sensors. Our result partially supports the hypothesis during level walking, where only the knee and ankle joints saw significant improvements ( $p < 0.05$ ) in joint work correlations with added sound-side sensing over prosthesis-side only sensing. For the hip joints, we were not able to conclude any significant advantages with the additional sensors. These results additionally support our hypothesis that joints further away would benefit from the added sensing, as only the ankle and knee joints saw improved correlation values. To more accurately estimate the sound-side joint work for prosthesis users, having additional sensors on the sound-side is advantageous, but if we are only concerned about estimating hip work, it may not be necessary.

During level walking, results showed certain joints had overall higher correlations than others, where the ankle yielded the best estimates, then hip, and finally knee. This shows that in general, the more contribution a particular joint has in a specific ambulation mode [], the easier it is to detect changes in the joint work. Similarly in the ramp descent trials, the model was struggling to accurately detect work trends in the ankle and hip, while the knee joint had higher joint work correlation because of the more definitive power curve profile.

When incorporating sound sensing for improved joint work estimations, it was hypothesized that including all possible sound-side sensors would yield the best results. However, our results show that such is not necessarily the case as we did not see significant differences ( $p < 0.05$ ) between using all sensors and smaller subsets of sensors. In level walking, it is enough to have just the insole and tibia IMU to accurately measure joint work values. Because these two sensors surround the ankle joint, they most likely hold the essential joint information necessary to accurately measure ankle joint dynamics. And because the ankle is a dominant joint during level walking, the effects of these sensors could translate to the other joints.

Comparing ramp trials, the model's estimations for ramp ascent and level walking showed similar trends across joints, with no significant differences ( $p > 0.05$ ). This is expected due to similar biomechanics, but ramp ascent requires more positive work, particularly from the knee, resulting in better knee joint work correlations. In contrast, the model performed poorly on ramp descent for the ankle and hip joints because the biomechanics of ramp descent are quite different from level walking and ramp ascent, and the training set is oversaturated with level walking data. In addition, as the subject walks down the ramp, they must actively control and decelerate the body, and such movements can typically be associated with higher variability and less smooth force production compared to a push-off motion during ramp ascent [58]. There may also be greater variability in foot placement while descending a ramp to maintain balance and prevent falls, and greater impact forces due to the gravitational pull [60]. On the other hand, ramp ascent may exhibit more consistent and controlled signals as maintaining stability is not as challenging. The CNN models used were the same as those for level walking, so a properly

optimized model for each task and label may be able to improve the model significantly as well. But even despite that, both models were able to portray meaningful trends. The model accurately detected larger joint power magnitudes in the knee during, which is more dominant during ramp descent. This indicates that the model's performance varies with the relative contribution of each joint in different ambulation modes.

In general, the results on ramp did not support our hypothesis as adding sound-side sensors did not improve joint work estimations, apart from the sound-side ankle. This may not necessarily mean sound-side sensors hurt joint work estimations during ramp locomotion, but rather allude to poor sensor simulation on the collected ramp data. While the user is spatially stationary during level walking as they ambulate on a treadmill, during ramps the user is dynamically moving throughout the terrain park, which may result in noisier VICON motion capture data with larger marker gaps. This error can propagate through the biomechanics processing pipeline and generate inaccurate and high variance simulated IMU data.

This thesis also explored the various ML models for estimating joint work. Similar to other works that have successfully estimated joint moment in real-time, one of the approaches was estimating the power curve and then integrating for work, while the other was to try predicting the work term directly without the need for integration. Results from section 4.1 showed that the CNN in general was a better choice over a TCN, a more recent deep-learning model that can capture temporal elements in time-series data effectively [38-40]. Although the literature has shown the TCN to outperform the CNN with certain scenarios [38-40], one of the potential reasons that it was not so successful for this thesis was that the amount of data may not have been enough for the TCN to accurately capture

temporal elements. This is evident given that the variation seen in not only the TCN predictions but also the CNN predictions, is quite large. While general qualitative analyses of the model performances are captured well to see relative results, seven subjects' worth of data may be the reason why statistical analyses showed p-values close to 0.05, but not significant enough.

When strictly comparing the performances of CNN-power to CNN-work, the latter does seem to have an edge when it comes to estimating joint work for the hip joints. The CNN-work also has the advantage of computational efficiency because it can look at the full gait cycle to make a prediction, while the CNN-power relies on a sliding window that only captures segments of the gait cycle at a time. However, the analyses done from section 4.3 onwards mainly work with CNN-power because it was deemed to be more reliable. Given that we are working on a limited dataset, the sliding window gives significantly larger data to train with compared to having one label per gait cycle, thus reducing the variability in the data. Provided that there are more subject data, the CNN-work has the potential to outperform the CNN-power, and it may be more suitable for real-time implementations as well.

For many of the results, the ankle joint tends to have better estimations and correlations compared to the other joints, specifically within level walking. One potential reason could be due to the way the models were optimized. All models used in this thesis were single output models, meaning they were trained and tested with just a single joint label, rather than estimating for all joints at once. This is because the three joints may have very distinct patterns that may be challenging for the model to capture simultaneously. As a result, during the model optimization process, the model for estimating the ankle moment

was mainly used. It is difficult to prove that such is the case without optimizing the model for each label but given that the model can reach relatively low variability with hip and knee joints, the main reason may be that certain joints are easier to estimate than others. For example, sections 4.1 through 4.3 show an overall bad estimate of the knee joint during level walking. This can result from the fact that during level walking the dominant joints are the hip and ankle, with the knee having little contribution. As a result, the relative joint power values are much lower, and because the model integrates the power curve, the relative errors can become large causing the correlation to be difficult to capture. On top of that, the weak patterns can increase the variability across subjects. Conversely, that is why results from the ramp models show significantly better estimates for the knee joint; during ramp trials, the knee generates and absorbs more energy, creating a distinct pattern in the sensor signals that makes it easier for the ML models to capture and predict.

## CHAPTER 6: CONCLUSION AND FUTURE WORK

By estimating joint work on the sound side in relation to the prosthetic side, this study addresses a significant gap in the field by creating and validating a pipeline for accurate joint work estimation, a task not previously achieved. This approach offers several benefits: it eliminates the need for costly and time-consuming motion capture or force plates, provides a method of real-time feedback for optimizing prosthetic control, and delivers biofeedback to help individuals with amputations develop healthier gait patterns. Real-time assessment of joint work symmetry between the prosthetic and intact limb can highlight gait anomalies, such as increased joint power at a constant speed and terrain, prompting adjustments in prosthetic assistance to improve gait balance. Furthermore, comparing prosthetic-induced joint work to natural limb dynamics and fine-tuning prosthetic assistance can potentially reducing the risk of joint issues like osteoarthritis. Overall, this pipeline enables regular monitoring and early intervention to prevent maladaptive gait patterns and support long-term joint health in lower-limb amputees.

One of the main improvements to the study is collecting more data to improve the overall results. While we were able to capture general trends in joint work within different modes and sensor configurations, the small dataset made it difficult to form statistically significant differences ( $p < 0.05$ ) between the results due to the large variance seen across subjects. Specifically for CNN-work, each gait cycle provides only one datapoint as opposed to hundreds of sliding windows for the power integration method. The drastically smaller dataset may be a reason to why the CNN-work model was not able to show significant results when compared to the other models despite showing qualitatively better

correlation values in certain joints. Similarly, the TCN was seen to overfit to the training set during training due to lack of data.

It would also be important to explore a more thorough optimization of the presented models. The model was primarily optimized over the ankle joint which may have resulted in slightly poor performances on the other joints compared to the sound-side ankle. If each model was fully optimized for the joints individually, the variability in the results would improve. Similarly, the TCN model used was optimized for joint moments in able-bodied users, which may have been the reason behind its low correlation results. Exploration of other ML models would be worthwhile, especially for direct work calculations. Because a CNN depends on a fixed window size, each gait sequence had to be modified to have a universal length. Such a transformation may impact the way the data is interpreted, so attempting a model that can accept variable input sizes and lengths may be beneficial. While this study explored the expansion into ramp walking, other modes of ambulation may be worth exploring as well, especially stair ascent and descent. It would be intriguing to see how the model performs on stairs as it has more dynamic biomechanics than level walking or ramps.

## REFERENCES

- [1] P. F. Pasquina, A. J. Carvalho and T. P. Sheehan, "Ethics in rehabilitation: Access to prosthetics and Quality Care following amputation", *AMA Journal of Ethics*, vol. 17, no. 6, pp. 535-546, 2015.
- [2] A. Domínguez-Ruiz et al., "Low limb prostheses and complex human prosthetic interaction: A systematic literature review," *Frontiers in Robotics and AI*, vol. 10. Frontiers Media SA, Feb. 13, 2023. doi: 10.3389/frobt.2023.1032748.
- [3] E. Lathouwers et al., "Therapeutic benefits of lower limb prostheses: a systematic review," *Journal of NeuroEngineering and Rehabilitation*, vol. 20, no. 1. Springer Science and Business Media LLC, Jan. 13, 2023. doi: 10.1186/s12984-023-01128-5.
- [4] A. Chadwell et al., "Technology for monitoring everyday prosthesis use: a systematic review," *Journal of NeuroEngineering and Rehabilitation*, vol. 17, no. 1. Springer Science and Business Media LLC, Jul. 14, 2020. doi: 10.1186/s12984-020-00711-4.
- [5] M. Schaarschmidt, S. W. Lipfert, C. Meier-Gratz, H.-C. Scholle, and A. Seyfarth, "Functional gait asymmetry of unilateral transfemoral amputees," *Human Movement Science*, vol. 31, no. 4. Elsevier BV, pp. 907–917, Aug. 2012. doi: 10.1016/j.humov.2011.09.004.
- [6] P. G. Adamczyk and A. D. Kuo, "Mechanisms of Gait Asymmetry Due to Push-Off Deficiency in Unilateral Amputees," *IEEE Transactions on Neural Systems and Rehabilitation Engineering*, vol. 23, no. 5. Institute of Electrical and Electronics Engineers (IEEE), pp. 776–785, Sep. 2015. doi: 10.1109/tnsre.2014.2356722.
- [7] R. D. Wedge, F. C. Sup IV, and B. R. Umberger, "Metabolic cost of transport and stance time asymmetry in individuals with unilateral transtibial amputation using a passive prostheses while walking," *Clinical Biomechanics*, vol. 94. Elsevier BV, p. 105632, Apr. 2022. doi: 10.1016/j.clinbiomech.2022.105632.
- [8] K. K. Patterson et al., "Gait Asymmetry in Community-Ambulating Stroke Survivors," *Archives of Physical Medicine and Rehabilitation*, vol. 89, no. 2. Elsevier BV, pp. 304–310, Feb. 2008. doi: 10.1016/j.apmr.2007.08.142.

- [9] M. L. Callisaya et al., “Gait, gait variability and the risk of multiple incident falls in older people: a population-based study,” *Age and Ageing*, vol. 40, no. 4. Oxford University Press (OUP), pp. 481–487, May 31, 2011. doi: 10.1093/ageing/afr055.
- [10] S. Nadeau, “Understanding Spatial and Temporal Gait Asymmetries in Individuals Post Stroke,” *International Journal of Physical Medicine & Rehabilitation*, vol. 02, no. 03. OMICS Publishing Group, 2014. doi: 10.4172/2329-9096.1000201.
- [11] A. S. Göktepe, B. Cakir, B. Yilmaz, and K. Yazicioglu, “Energy Expenditure of Walking with Prostheses,” *Prosthetics & Orthotics International*, vol. 34, no. 1. Ovid Technologies (Wolters Kluwer Health), pp. 31–36, Mar. 2010. doi: 10.3109/03093640903433928.
- [12] T. Schmalz, S. Blumentritt, and R. Jarasch, “Energy expenditure and biomechanical characteristics of lower limb amputee gait:,” *Gait & Posture*, vol. 16, no. 3. Elsevier BV, pp. 255–263, Dec. 2002. doi: 10.1016/s0966-6362(02)00008-5.
- [13] M. Grimmer et al., “A powered prosthetic ankle joint for walking and running,” *BioMedical Engineering OnLine*, vol. 15, no. S3. Springer Science and Business Media LLC, Dec. 2016. doi: 10.1186/s12938-016-0286-7.
- [14] A. E. Ferris, J. M. Aldridge, C. A. Rábago, and J. M. Wilken, “Evaluation of a Powered Ankle-Foot Prosthetic System During Walking,” *Archives of Physical Medicine and Rehabilitation*, vol. 93, no. 11. Elsevier BV, pp. 1911–1918, Nov. 2012. doi: 10.1016/j.apmr.2012.06.009.
- [15] Q. Li, S. Chen, C. Xu, X. Chu, and Z. Li, “Design, Control and Implementation of a Powered Prosthetic Leg,” 2018 11th International Workshop on Human Friendly Robotics (HFR). IEEE, Nov. 2018. doi: 10.1109/hfr.2018.8633466.
- [16] A. J. Young, A. M. Simon, N. P. Fey, and L. J. Hargrove, “Intent Recognition in a Powered Lower Limb Prosthesis Using Time History Information,” *Annals of Biomedical Engineering*, vol. 42, no. 3. Springer Science and Business Media LLC, pp. 631–641, Sep. 20, 2013. doi: 10.1007/s10439-013-0909-0.
- [17] L. J. Hargrove et al., “Intuitive Control of a Powered Prosthetic Leg During Ambulation,” *JAMA*, vol. 313, no. 22. American Medical Association (AMA), p. 2244, Jun. 09, 2015. doi: 10.1001/jama.2015.4527.

- [18] M. J. Highsmith, J. T. Kahle, D. R. Bongiorno, B. S. Sutton, S. Groer, and K. R. Kaufman, "Safety, Energy Efficiency, and Cost Efficacy of the C-Leg for Transfemoral Amputees," *Prosthetics & Orthotics International*, vol. 34, no. 4. Ovid Technologies (Wolters Kluwer Health), pp. 362–377, Dec. 2010. doi: 10.3109/03093646.2010.520054.
- [19] M. Tran, L. Gabert, M. Cempini, and T. Lenzi, "A Lightweight, Efficient Fully Powered Knee Prosthesis With Actively Variable Transmission," *IEEE Robotics and Automation Letters*, vol. 4, no. 2. Institute of Electrical and Electronics Engineers (IEEE), pp. 1186–1193, Apr. 2019. doi: 10.1109/lra.2019.2892204.
- [20] S. K. Au, J. Weber, and H. Herr, "Powered Ankle--Foot Prosthesis Improves Walking Metabolic Economy," *IEEE Transactions on Robotics*, vol. 25, no. 1. Institute of Electrical and Electronics Engineers (IEEE), pp. 51–66, Feb. 2009. doi: 10.1109/tro.2008.2008747.
- [21] L. J. Hargrove et al., "Robotic Leg Control with EMG Decoding in an Amputee with Nerve Transfers," *New England Journal of Medicine*, vol. 369, no. 13. Massachusetts Medical Society, pp. 1237–1242, Sep. 26, 2013. doi: 10.1056/nejmoa1300126.
- [22] H. A. Varol and Y. Massalin, "A feasibility study of depth image based intent recognition for lower limb prostheses," 2016 38th Annual International Conference of the IEEE Engineering in Medicine and Biology Society (EMBC). IEEE, Aug. 2016. doi: 10.1109/embc.2016.7591863.
- [23] M. Pi, "Gait Control of Robotic Leg Prosthesis Based on Motion Predictive System," 2020 5th International Conference on Advanced Robotics and Mechatronics (ICARM). IEEE, Dec. 2020. doi: 10.1109/icarm49381.2020.9195310.
- [24] S. Cheng, C. A. Laubscher, and R. D. Gregg, "Automatic Stub Avoidance for a Powered Prosthetic Leg Over Stairs and Obstacles," *IEEE Transactions on Biomedical Engineering*, vol. 71, no. 5. Institute of Electrical and Electronics Engineers (IEEE), pp. 1499–1510, May 2024. doi: 10.1109/tbme.2023.3340628.
- [25] K. Zhang et al., "Environmental Features Recognition for Lower Limb Prostheses Toward Predictive Walking," *IEEE Transactions on Neural Systems and Rehabilitation Engineering*, vol. 27, no. 3. Institute of Electrical and Electronics Engineers (IEEE), pp. 465–476, Mar. 2019. doi: 10.1109/tnsre.2019.2895221.

- [26] M. T. Farrell and H. Herr, "A method to determine the optimal features for control of a powered lower-limb prostheses," 2011 Annual International Conference of the IEEE Engineering in Medicine and Biology Society. IEEE, Aug. 2011. doi: 10.1109/iembs.2011.6091493.
- [27] G. Khademi and D. Simon, "Toward Minimal-Sensing Locomotion Mode Recognition for a Powered Knee-Ankle Prosthesis," *IEEE Transactions on Biomedical Engineering*, vol. 68, no. 3. Institute of Electrical and Electronics Engineers (IEEE), pp. 967–979, Mar. 2021. doi: 10.1109/tbme.2020.3016129.
- [28] J. A. Spanias, A. M. Simon, S. B. Finucane, E. J. Perreault, and L. J. Hargrove, "Online adaptive neural control of a robotic lower limb prosthesis," *Journal of Neural Engineering*, vol. 15, no. 1. IOP Publishing, p. 016015, Jan. 09, 2018. doi: 10.1088/1741-2552/aa92a8.
- [29] C. Johnson, J. Cho, J. Maldonado-Contreras, S. Chaluvadi, and A. J. Young, "Adaptive Lower-Limb Prosthetic Control: Towards Personalized Intent Recognition & Context Estimation," 2023 International Symposium on Medical Robotics (ISMR). IEEE, Apr. 19, 2023. doi: 10.1109/ismr57123.2023.10130251.
- [30] J. Y. Maldonado-Contreras, K. Bhakta, J. Camargo, P. Kunapuli, and A. J. Young, "User- and Speed-Independent Slope Estimation for Lower-Extremity Wearable Robots," *Annals of Biomedical Engineering*, vol. 52, no. 3. Springer Science and Business Media LLC, pp. 487–497, Nov. 06, 2023. doi: 10.1007/s10439-023-03391-y.
- [31] K. Bhakta et al., "Continuous-Context, User-Independent, Real-Time Intent Recognition for Powered Lower-Limb Prostheses." Georgia Institute of Technology, 2023. doi: 10.35090/GATECH/70300.
- [32] T. Chen and C. Guestrin, "XGBoost: A Scalable Tree Boosting System," arXiv, 2016, doi: 10.48550/ARXIV.1603.0277.
- [33] K. O'Shea and R. Nash, "An Introduction to Convolutional Neural Networks." arXiv, 2015. doi: 10.48550/ARXIV.1511.08458.
- [34] S. Hochreiter and J. Schmidhuber, "Long Short-Term Memory," *Neural Computation*, vol. 9, no. 8. MIT Press, pp. 1735–1780, Nov. 01, 1997. doi: 10.1162/neco.1997.9.8.1735.

- [35] S. Bai, J. Z. Kolter, and V. Koltun, “An Empirical Evaluation of Generic Convolutional and Recurrent Networks for Sequence Modeling.” arXiv, 2018. doi: 10.48550/ARXIV.1803.01271.
- [36] K. Bhakta, J. Camargo, W. Compton, K. Herrin, and A. Young, “Evaluation of Continuous Walking Speed Determination Algorithms and Embedded Sensors for a Powered Knee & Ankle Prosthesis,” *IEEE Robotics and Automation Letters*, vol. 6, no. 3. Institute of Electrical and Electronics Engineers (IEEE), pp. 4820–4826, Jul. 2021. doi: 10.1109/lra.2021.3068711.
- [37] J. Camargo, W. Flanagan, N. Csomay-Shanklin, B. Kanwar, and A. Young, “A Machine Learning Strategy for Locomotion Classification and Parameter Estimation Using Fusion of Wearable Sensors,” *IEEE Transactions on Biomedical Engineering*, vol. 68, no. 5. Institute of Electrical and Electronics Engineers (IEEE), pp. 1569–1578, May 2021. doi: 10.1109/tbme.2021.3065809.
- [38] D. D. Molinaro, I. Kang, and A. J. Young, “Estimating human joint moments unifies exoskeleton control, reducing user effort,” *Science Robotics*, vol. 9, no. 88. American Association for the Advancement of Science (AAAS), Mar. 20, 2024. doi: 10.1126/scirobotics.adi8852.
- [39] K. Scherpereel, D. Molinaro, O. Inan, M. Shepherd, and A. Young, “A human lower-limb biomechanics and wearable sensors dataset during cyclic and non-cyclic activities,” *Scientific Data*, vol. 10, no. 1. Springer Science and Business Media LLC, Dec. 21, 2023. doi: 10.1038/s41597-023-02840-6.
- [40] D. D. Molinaro, I. Kang, J. Camargo, M. C. Gombolay, and A. J. Young, “Subject-Independent, Biological Hip Moment Estimation During Multimodal Overground Ambulation Using Deep Learning,” *IEEE Transactions on Medical Robotics and Bionics*, vol. 4, no. 1. Institute of Electrical and Electronics Engineers (IEEE), pp. 219–229, Feb. 2022. doi: 10.1109/tmrb.2022.3144025.
- [41] X. Jiang, M. Gholami, M. Khoshnam, J. J. Eng, and C. Menon, “Estimation of Ankle Joint Power during Walking Using Two Inertial Sensors,” *Sensors*, vol. 19, no. 12. MDPI AG, p. 2796, Jun. 21, 2019. doi: 10.3390/s19122796.
- [42] S. M. Moghadam, T. Yeung, and J. Choisne, “A comparison of machine learning models’ accuracy in predicting lower-limb joints’ kinematics, kinetics, and muscle forces from wearable sensors,” *Scientific Reports*, vol. 13, no. 1. Springer Science and Business Media LLC, Mar. 28, 2023. doi: 10.1038/s41598-023-31906-z.

- [43] H. Jin, I. Kang, G. Choi, D. D. Molinaro, and A. J. Young, “Wearable Sensor-Based Step Length Estimation During Overground Locomotion Using a Deep Convolutional Neural Network,” 2021 43rd Annual International Conference of the IEEE Engineering in Medicine & Biology Society (EMBC). IEEE, Nov. 01, 2021. doi: 10.1109/embc46164.2021.9630060.
- [44] B. L. Fylstra, I.-C. Lee, M. Li, M. D. Lewek, and H. Huang, “Human-prosthesis cooperation: combining adaptive prosthesis control with visual feedback guided gait,” *Journal of NeuroEngineering and Rehabilitation*, vol. 19, no. 1. Springer Science and Business Media LLC, Dec. 14, 2022. doi: 10.1186/s12984-022-01118-z.
- [45] Y. Feng, C. Mao, and Q. Wang, “Gait-symmetry-based human-in-the-loop optimization for unilateral transtibial amputees with robotic prostheses.” Cold Spring Harbor Laboratory, Oct. 05, 2020. doi: 10.1101/2020.10.04.325720.
- [46] J. B. Dingwell, B. L. Davis, and D. M. Frazder, “Use of an instrumented treadmill for real-time gait symmetry evaluation and feedback in normal and trans-tibial amputee subjects,” *Prosthetics & Orthotics International*, vol. 20, no. 2. Ovid Technologies (Wolters Kluwer Health), pp. 101–110, Aug. 1996. doi: 10.3109/03093649609164426.
- [47] E. R. C. Draper, “A treadmill-based system for measuring symmetry of gait,” *Medical Engineering & Physics*, vol. 22, no. 3. Elsevier BV, pp. 215–222, Apr. 2000. doi: 10.1016/s1350-4533(00)00026-6.
- [48] Ming-Yih Lee, Chih Feng Lin, and Kok Soon Soon, “Balance control enhancement using sub-sensory stimulation and visual-auditory biofeedback strategies for amputee subjects,” 2007 IEEE International Conference on Systems, Man and Cybernetics. IEEE, 2007. doi: 10.1109/icsmc.2007.4414064.
- [49] A. F. Azocar, L. M. Mooney, J.-F. Duval, A. M. Simon, L. J. Hargrove, and E. J. Rouse, “Design and clinical implementation of an open-source bionic leg,” *Nature Biomedical Engineering*, vol. 4, no. 10. Springer Science and Business Media LLC, pp. 941–953, Oct. 05, 2020. doi: 10.1038/s41551-020-00619-3.
- [50] K. Bhakta, J. Camargo, P. Kunapuli, L. Childers, and A. Young, “Impedance Control Strategies for Enhancing Sloped and Level Walking Capabilities for Individuals with Transfemoral Amputation Using a Powered Multi-Joint Prosthesis,” *Military Medicine*, vol. 185, no. Supplement\_1. Oxford University Press (OUP), pp. 490–499, Dec. 09, 2019. doi: 10.1093/milmed/usz229.

- [51] A. M. Simon et al., “Configuring a Powered Knee and Ankle Prosthesis for Transfemoral Amputees within Five Specific Ambulation Modes,” *PLoS ONE*, vol. 9, no. 6. Public Library of Science (PLoS), p. e99387, Jun. 10, 2014. doi: 10.1371/journal.pone.0099387.
- [52] S. L. Delp et al., “OpenSim: Open-Source Software to Create and Analyze Dynamic Simulations of Movement,” *IEEE Transactions on Biomedical Engineering*, vol. 54, no. 11. Institute of Electrical and Electronics Engineers (IEEE), pp. 1940–1950, Nov. 2007. doi: 10.1109/tbme.2007.901024.
- [53] J. Camargo, K. Bhakta, J. Maldonado-Contreras, S. Zhou, K. Herrin, and A. Young, “OpenSim Model for Biomechanical Analysis with the Open-Source Bionic Leg,” 2022 International Symposium on Medical Robotics (ISMR). IEEE, Apr. 13, 2022. doi: 10.1109/ismr48347.2022.9807551.
- [54] K. Scherpereel, D. Molinaro, O. Inan, M. Shepherd, and A. Young, “A human lower-limb biomechanics and wearable sensors dataset during cyclic and non-cyclic activities,” *Scientific Data*, vol. 10, no. 1. Springer Science and Business Media LLC, Dec. 21, 2023. doi: 10.1038/s41597-023-02840-6.
- [55] M. Bodini, “Aspect Extraction from Bangla Reviews Through Stacked Auto-Encoders,” *Data*, vol. 4, no. 3. MDPI AG, p. 121, Aug. 09, 2019. doi: 10.3390/data4030121.
- [56] C. Huang, N. Du, J. He, N. Li, Y. Feng, and W. Cai, “Multidimensional Feature-Based Graph Attention Networks and Dynamic Learning for Electricity Load Forecasting,” *Energies*, vol. 16, no. 18. MDPI AG, p. 6443, Sep. 06, 2023. doi: 10.3390/en16186443.
- [57] C. Pham, L. Nguyen, A. Nguyen, N. Nguyen, and V.-T. Nguyen, “Combining skeleton and accelerometer data for human fine-grained activity recognition and abnormal behaviour detection with deep temporal convolutional networks,” *Multimedia Tools and Applications*, vol. 80, no. 19. Springer Science and Business Media LLC, pp. 28919–28940, Jun. 15, 2021. doi: 10.1007/s11042-021-11058-w.
- [58] J. R. Montgomery and A. M. Grabowski, “The contributions of ankle, knee and hip joint work to individual leg work change during uphill and downhill walking over a range of speeds,” *Royal Society Open Science*, vol. 5, no. 8. The Royal Society, p. 180550, Aug. 2018. doi: 10.1098/rsos.180550.

- [59] J. Camargo, A. Ramanathan, W. Flanagan, and A. Young, “A comprehensive, open-source dataset of lower limb biomechanics in multiple conditions of stairs, ramps, and level-ground ambulation and transitions,” *Journal of Biomechanics*, vol. 119. Elsevier BV, p. 110320, Apr. 2021. doi: 10.1016/j.jbiomech.2021.110320.
- [60] V. Struchkov and J. G. Buckley, “Biomechanics of ramp descent in unilateral trans-tibial amputees: Comparison of a microprocessor controlled foot with conventional ankle-foot mechanisms,” *Clinical Biomechanics*, vol. 32. Elsevier BV, pp. 164–170, Feb. 2016. doi: 10.1016/j.clinbiomech.2015.11.015.